공학박사 학위논문

Cost-efficient and Practical Indoor Localization System Using Magnetic Fingerprint

지자기 지문을 이용한 비용 효율적이고 실용적인 실내 측위 시스템

2020년 2월

서울대학교 대학원

전기.컴퓨터공학부

곽 명 철

공학박사 학위논문

Cost-efficient and Practical Indoor Localization System Using Magnetic Fingerprint

지자기 지문을 이용한 비용 효율적이고 실용적인 실내 측위 시스템

2020년 2월

서울대학교 대학원

전기.컴퓨터공학부

곽 명 철

지자기 지문을 이용한 비용 효율적이고 실용적인 실내 측위 시스템

Cost-efficient and Practical Indoor Localization System Using Magnetic Fingerprint

지도교수 권 태 경

이 논문을 공학박사 학위논문으로 제출함

2019년 11월

서울대학교 대학원

전기.컴퓨터공학부

곽 명 철

곽 명 철의 박사 학위논문을 인준함

2019년 12월

위 원 장	김 종 권
부위원장	권 태 경
위 원	최 양 희
위 원	이 영 기
위 원	최 린

Abstract

Cost-efficient and Practical Indoor Localization System Using Magnetic Fingerprint

Myeongcheol Kwak
Department of Electrical Engineering & Computer Science
The Graduate School
Seoul National University

Over the decades, indoor localization system has been widely studied in the academic and also in the industrial area. Many sensors or wireless signals such as WiFi, Bluetooth, and inertial sensors are available when designing an indoor localization system, but among them, the systems using the geomagnetic field has advantages concerning accuracy and stability. Every spatial point in an indoor space has its own distinct and stable fingerprint, which arises owing to the distortion of the magnetic field induced by the surrounding steel and iron structures. The magnetic fingerprint is robust to environmental changes like pedestrian activities and door/window movements, particularly compared with radio signals such as WiFi. This phenomenon makes many indoor positioning

techniques rely on the magnetic field as an essential source of localization.

Despite the robustness, there are some challenges when leveraging the magnetic fingerprint to design the indoor localization system. Due to lower discernibility of the magnetic fingerprint, most of the existing studies have exploited high computational algorithms and many sensors. Also, the cost of a site survey to collect the fingerprints and periodic management of target spaces is still problematic when using magnetic fingerprints. This dissertation thus focuses on these two challenges.

First, we present an energy-efficient and lightweight system that utilizes the magnetic field for indoor positioning in the Internet of Things (IoT) environments. We propose a new hardware design of an IoT device that only has a BLE interface and two sensors (magnetometer and accelerometer), with the lifetime of one year when using a coin-size battery. We further propose an augmented particle filter framework that features a robust motion model and algorithmic-efficient localization heuristics with minimal sensory data. The prototype-based evaluation shows that the proposed system achieves a median accuracy of 1.62 m for an office building while exhibiting low computational complexity and high energy efficiency.

Next, we propose a magnetic fingerprint-based indoor localization system leveraging a crowdsourcing approach. In the aspect of indoor localization, crowdsourcing is a method to construct the fingerprint database without the explicit site-survey process. Over the past decade, crowdsourcing has been actively studied for indoor localization. However, the existing localization systems based on crowdsourcing usually achieve lower location accuracy than the site survey based systems. To overcome the low performance of the crowdsourcing based approaches, we design an indoor positioning system using the crowdsourced data of the magnetic field. We substantiate a novel HMM-based learning model

to construct a database of magnetic field fingerprints from smartphone users. Experiments in an indoor space consisting of aisles show that the proposed system achieves the learning accuracy of 96.47% and median positioning accuracy of 0.25m.

Keywords: Indoor Localization, Internet of Things (IoT), Magnetic Field, Mobile Computing, Augmented Particle Filter, Hidden Markov Model
Student Number: 2012-20733

Contents

List of Figures

List of Tables

Chapter 1

Introduction

1.1 Motivation

Location-Based Service (LBS) and its applications such as navigation, commercial advertisement based on geofencing, and emergency escape services have become familiar to people in real life. To provide a such location-based service, the technologies to infer the user's location is essential. However, in the indoor space, it is not possible to leverage the widely used GPS based positioning technology since the GPS signals are blocked by building walls. Therefore, technologies to estimate the user's location in indoor space have been continuously researched, replacing GPS technology. As has been widely known, various types of data such as wireless signal, sensor data from inertial sensors including accelerometer and gyroscope, and magnetic sensor can be used to construct an indoor positioning system [1, 6, 35, 37]. Each data has the advantages and disadvantages when designing an indoor positioning system, and there typically is a trade-off relationship between cost and accuracy. Among them, magnetic

sensor data, in particular, has been noted as a practical alternative, thanks to its stability and efficiency.

The magnetic distortion occurred by a steel structure in an indoor space creates a characteristic magnetic pattern in each space. Although this phenomenon acts as a disadvantage when inferring the direction of the user when using the magnetic sensor as a compass, it can also be used as a promising localization technology by leveraging a method that records magnetic patterns as a fingerprint [2, 5, 6]. Since the magnetic pattern in each space does not change as long as the structure of the building significantly changes and the human body does not interfere with it, the magnetic fingerprinting method is not only stable and robust, but it also does not cost much to collect [2].

1.2 Indoor Localization Overview

There have been many attempts to use various types of data to design an indoor positioning system. Whichever we choose the data for indoor positioning, there is typically a trade-off relationship between cost and accuracy, but the magnetic field based localization system has some advantages in practical terms when considering trade-offs between costs and accuracy, as shown in Figure 1.1. In this section, I describe the proposed indoor localization systems based on various types of data to compare them with magnetic based systems.

WiFi based systems: Since RADAR [1] proposed a fingerprinting method that estimates the user's location by recording WiFi signals by space, many techniques have been proposed to leverage WiFi signals for indoor positioning. HORUS [21] proposed a method that increases the accuracy of the fingerprinting technique by clustering between similar signals and probabilistic matching, and FreeLoc [20] proposed a more reliable system by introducing a robust finger-

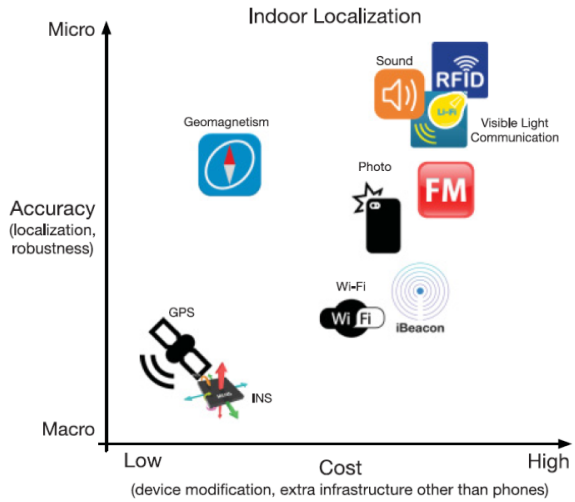

Figure 1.1 Comparison of different data for indoor localization concerning the trade-off relationship between cost and accuracy [16].

print model regardless environmental changes and device diversity issue. WiFi fingerprinting method based systems use WiFi AP, which is a widely deployed infrastructure, so they do not require much deployment cost and provide a level of accuracy of less than 5m with a relatively simple algorithm. However, due to the nature of wireless signals with frequent fluctuation by interference such as the human body, the variability of accuracy is also high, and the cost of periodic recollection is wasted since the WiFi fingerprint changes over time. Systems such as CUPID [45] proposed a trilateration based positioning system using the measurement of the distance between WiFi APs and a user. Leveraging this approach saves on the cost of preliminary site-survey, but it costs a dedicated WiFi AP and device, and even a wireless protocol.

UWB based systems: UWB (Ultrawide-band) has wide bandwidth and short durations, so it is robust to signal interference and multipath effects. These characteristics are suitable for designing an indoor positioning system with very

high accuracy. Systems such as [37, 38] proposed UWB based indoor positioning techniques that would work under NLOS (Non-Line-of-Sight) scenario, and their level of accuracy is centimeter level. However, they still need a cost for deployment of dedicated devices and complicated algorithms for time synchronization and multipath mitigation.

Visible light based systems: The use of visible light for indoor positioning is a recently popular approach. These systems, such as [43, 44], achieve high accuracy in the centimeter level by using fluorescent patterns everywhere in the interior, so they do not require high deployment costs. However, requiring a LOS (Line-of-Sight) path between the device and the fluorescent lamp for system operation and a high algorithmic cost for frequent camera operation and image analysis are still research challenges.

Inertial sensor based systems: Inertial sensors usually stand for accelerometers, gyroscopes, and magnetic sensors. In the aspects of indoor localization, we can primarily leverage them for PDR (Pedestrian Dead Reckoning), which infers the number of steps and heading direction by detecting sensor patterns that occur during a user's walk. Systems such as [3, 4] leveraged inertial sensors for indoor positioning, show low accuracy when used alone since 1) the PDR technique itself can only identify the relative path from the previous position, and 2) the magnetic sensor operated as a compass may malfunction due to the phenomenon of magnetic distortion in indoor space, resulting in severe positioning errors. Therefore, inertial sensor based localization techniques are usually used as a complementary role by fusing with other data for positioning (i.e., WiFi).

1.3 Magnetic Field based Systems

As claimed in [2, 27], a space-specific magnetic pattern caused by magnetic distortion in indoor space is not interfered by the movement of human beings and other obstacles in real life, and do not change over a long period unless the structure of the building changes significantly. Figure 2.1(b) depicts the stable phenomenon of the magnetic field patterns, which is collected on the same corridor from different devices.

Also, the magnetic field sensor does not require the LOS path obtained since it reads the magnetic pattern in the indoor space itself without a particular transmission node such as WiFi AP. From a cost perspective, we can easily collect the magnetic readings from anywhere on the earth without installation of any infrastructure, and unlike wireless signals or visual images, the magnetic sensor does not require much energy to obtain sensor values. These are significant advantages when designing an indoor positioning system concerning robustness, accuracy, and cost efficiency compared to the other data sources introduced in the previous sub-section.

However, since magnetic sensor reading is a three-dimensional time series data, it is essential to use the pattern of changes in sensor readings as a result of user movement, unlike other data sources with relatively many dimensions (i.e., many APs in a WiFi fingerprint). Also, to make the magnetic sensor readings robust to changes in the local coordinate system of the device, that depend on the user's walk or device holding position, we have to rotate the raw magnetic sensor readings to the global coordinate system. After the rotation to the global coordinate system based on the gravity plane and the direction of the magnetic pole, there are only two dimensions left in the magnetic sensor data. Against this backdrop, many techniques have been proposed over the last decades to

construct an accurate and cost-efficient indoor localization system using the magnetic field.

To the best of my knowledge, [24] first proposed a practical model of the magnetic field based indoor localization system. [24] defines the compass orientation error as a Compass Signature and estimates the position of the robot by recording and tracking it. Although the authors conducted the experiments in a very narrow space and the accuracy was not high due to the use of one-dimensional data, [24] was the first paper to propose a methodology for designing an indoor localization system using the magnetic field.

Systems such as [22, 23] propose a methodology for constructing an indoor positioning system using the three-dimensional raw magnetic sensor data. However, as explained before, the raw magnetic sensor reading is not robust to the changes in the device's coordinate system. Moreover, the pre-survey process for fingerprint collecting is too expensive since we have to collect all the magnetic patterns depending on the heading direction of the device or the user.

LocateMe [2] proposes the system using the amplitude of the magnetic field, based on a comprehensive analysis of the magnetic distortion model in indoor space and useful characteristics of the magnetic field for indoor localization. However, systems such as [2, 41] limited to space in the form of corridors since it introduces a methodology to record and compare the magnetic patterns in a long, unidimensional line. MaLoc [5] and Magicol [6] leverage a coordinate-transformed two-dimensional magnetic pattern to make the positioning algorithm robust to the changes in the device's coordinate system. Also, these systems introduce the particle filter framework as the positioning algorithm, enabling accurate positioning in various forms of two-dimensional indoor space. However, the high algorithmic complexity, as well as the low-level accuracy in open space in the form of a square, and the need for a dense level of site-survey

are still research challenges.

1.4 Organization of Dissertation

In the previous sections, this dissertation introduced research background and many academic attempts that have tried to leverage the magnetic field to design a localization system. We now present the result of our works on the magnetic field based indoor positioning technique. The rest of this dissertation is organized as follows. After introducing some research backgrounds concerning the indoor localization and the magnetic field based systems in Chapter 1, We describe our previous work, which implements the design of a small IoT board for a localization purpose and suggests an energy-efficient positioning system including the comprehensive modules in Chapter 2. The second work which introduces a crowdsourcing based system using the magnetic fingerprint then is given in Chapter 3, followed by discussions in Chapter 4 and concluding remarks in Chapter 5.

Chapter 2

An Energy-efficient and Lightweight Indoor Localization System for Internet-of-Things (IoT) Environments

2.1 Introduction

Location-based applications such as car navigation systems, restaurant recommendation systems, parking locators, and emergency escape services have significantly increased the quality of our daily life. The location of a user is key contextual information that is utilized by such location-based services (LBSs). However, in indoor environments, the location of a user cannot be easily acquired owing to the blockade of global positioning system (GPS) signals by building structures. Hence, over the last decade, many methods for indoor location detection have been proposed.

There have been many attempts to use various sources of information for indoor location detection. Methods that utilize WiFi signals [1, 21] are among

the most widely used ones. However, these methods require frequent WiFi scans that result in signification consumption of energy. In addition, fluctuations in the signal strength negatively affect the localization performance. Ultra-wideband (UWB) based methods [39, 40, 37] can be highly accurate. However, these methods require customized hardware devices for analyzing reflected signals. More practical solutions are based on inertial sensors and include magnetometers, accelerometers, and gyroscopes [3]. However, these solutions have their own limitations. For instance, a heading inference mechanism in pedestrian dead reckoning (PDR) [10] usually suffers from the distortion effect of steel materials on geo-magnetism.

The distortion effect of steel materials on a magnetic field is a double-edged sword. Since the magnetic distortion makes each spatial point distinct from others, it can serve as a fingerprint that helps localize any device with a magnetic sensor. As claimed in [8] and [2], magnetic fields exhibit desirable properties for indoor localization, e.g., temporal stability and insensitivity to moving nearby objects [6]. In addition, magnetic sensors are cheap and off-the-shelf everywhere. Consequently, many studies have proposed to use magnetic fields to a certain degree: a complete system [5, 6], a supplementary module [41, 42], or a combination with other sources [17, 18].

The main problem associated with using magnetic fields for fingerprinting is that their sensor data requires special processing. The raw sensor reading from a magnetometer is parameterized as a three-dimensional vector, which should be transformed to a scalar (i.e., the magnitude of the vector) or to a two-dimensional vector [27], to mitigate the effect of noise owing to the device's movement. Note that such movement affects the reference coordinates, not the magnetic field itself. To deal with this issue, Maloc [5] and Magicol [6] used a temporal change in the magnetic field (generated in the course of the user's

motion) as a fingerprint, and incorporated this measure into a particle filter framework. However, comparison of the temporal patterns of the magnetic field and processing of the particle filter technique is computationally expensive, and is feasible only with high-end devices such as smartphones. In other words, such solutions may not be used for low-end devices such as Internet of things (IoT) devices, unless the issues of high computation complexity and energy efficiency are resolved. An energy-efficient and lightweight indoor localization technique is essential for IoT device-based localization.

IoT devices are typically small, lightweight, and energy-efficient, and thus are easy to deploy or relocate, compared with smartphones or other dedicated localization devices (i.e., foot-mounted IMUs). If the performance of IoT device-based localization is sufficient for commercial-grade service, it can be a low-cost and energy-efficient alternative for many LBSs: supervising and tracking of assets and employees in office/factory environments, preventing workers from entering hazard zones, providing more precise geofencing services for patients or child care, and guiding emergency escape, to name a few.

To address these constraints and to reduce the cost of computation, we propose a novel magnetic field-based indoor localization system for IoT devices. We used energy saving wireless communication, bluetooth low energy (BLE), and report here a proprietary system that features a BLE interface and a magnetic sensor. We also streamlined the positioning algorithms to reduce the computational complexity while maintaining the localization accuracy. In summary, the present work makes the following contributions to the field of LBSs.

- To the best of our knowledge, ours is the first attempt to design a magnetic field-based, energy-efficient, and lightweight indoor localization system for IoT applications. The first-class requirement for IoT devices is energy effi-

ciency; hence, we tackle the algorithmic complexity and energy efficiency while maintaining the localization precision.

- In this work, we develop a specialized IoT device hardware (and the corresponding firmware) that substantiates energy-efficient localization (Section 2.4).

- To reduce the system complexity, we streamline the server-side localization algorithms, as well as the design of the end-user device, while maintaining localization performance comparable to those of state-of-the-art localization techniques (Section 2.5).

- Using sensor data that were collected over a period of three months, we demonstrate that our proposed system is energy-efficient, i.e., a single-coin battery can last for one year.

This paper is organized as follows. After reviewing some related work in Section 2.2, we discuss several issues associated with the use of magnetic fields in Section 2.3. In Section 2.4, we explain our design of an IoT device for magnetic field-based localization. Section 2.5 introduces the architecture of our system that supports energy-efficient and lightweight localization for IoT environments. We then evaluate the proposed system in Section 2.6, and discuss the practical issues in Section 4.

2.2 Related Work

Over the last decade, many efforts have been made to utilize changes in the magnetic field of an indoor environment for localization. [24] first exploited the disturbance of a magnetic compass reading for positioning of a robot subject to

some constraints. [22, 23] attempted to leverage raw magnetic field data to construct a magnetic fingerprint. However, the raw magnetic field data significantly change with the location and heading of a magnetic sensor. These techniques thus require magnetic sensors to be fixed in space, or require a high overhead of the site survey or wardriving. These limitations make it difficult to use these approaches for positioning of humans. Therefore, as argued in [2] and [27], the raw magnetic field data should be transformed to make the sensor data robust to changes in the users' position as they move. [2] and [9] proposed a magnetic fingerprinting scheme based on the magnetic field's intensity, which is a scalar.

However, these systems can only localize users that move in straight trajectories, such as corridors; they cannot be used in complex structured areas. The systems proposed in MaLoc [5] and Magicol [6] adopted a two-dimensional magnetic fingerprinting model suggested in [27]. As the variation in the magnetic field data increases, the corresponding location is more likely to be uniquely identified, which enhances the localization performance. They also chose a particle filter framework to adapt to the complexity of indoor environments. However, the adoption of the particle filter framework significantly increases the algorithmic complexity of the problem, which reduces the device's energy efficiency. We believe that methods to reduce the cost of the site survey and to reduce the complexity of the system's operation (e.g., dynamic time warping (DTW) [34]) have not been given due attention; this realization motivated us to design a proprietary system for commercial-grade services.

2.3 Issues on Using Magnetic Field

2.3.1 Characteristics of Magnetic Field

As claimed in [8], approaches that use sensory data and radio frequency

(RF) signals for indoor localization should have three desirable properties: time-invariance, spatial distinctiveness, and universality. The sensory data generated by magnetic fields have been accepted to have these properties [2, 5, 26]. In addition, these magnetic fields are not affected by human bodies or moving (non-metal) objects in indoor environments [6]. This is one of the outstanding advantages of using magnetic fields for indoor localization, compared with time-dependent RF signals such as WiFi.

Moreover, as explained in the previous section, the sensor data should be transformed to enhance the method's robustness with respect to changes in the position and heading of a magnetic sensor. The raw magnetic field data are parameterized as a three-dimensional vector, $B_{raw} = (B_x, B_y, B_z)$. As suggested in [27], it is possible to obtain a two-dimensional vector B_{hv} that consists of the horizontal component B_h and the vertical component B_v by rotating B_{raw} onto a gravity plane. Note that B_{hv} is hardly changed even if a magnetic sensor changes its position or heading due to a movement (e.g., the sensor holder's movement). That is why this transformation process is crucial when using the magnetic field for localization. While a two-dimensional vector form of a magnetic field for each spatial point is very helpful, it may not be sufficient for fine-grained localization, compared with WiFi fingerprinting that can be very high-dimensional. To overcome this phenomenon, [6] suggested to add another dimension to B_{hv} by accumulating the temporal history of B_{hv}, and use the temporal vector of B_{hv} as a magnetic fingerprint. We adopted the same approach in this paper.

2.3.2 Variation Issues

Even if the magnetic field in indoor environments is stable, actual sensor readings are somewhat complicated, owing to several reasons. First, different

magnetic sensors at the same location may show different readings, which can be owing to different manufacturing materials and/or different sensing mechanisms in these magnetic sensors. Figure 2.1(a) shows the magnetic sensor readings from three different devices over the same corridor (length, 60 m). Note that we plot only B_v for the sake of simplicity. The absolute differences between the readings of the three devices vary substantially, but their patterns of signal changes are similar. We can confirm this phenomenon by applying the mean removal technique to the individual patterns, as shown in Figure 2.1(b). The tendencies along the same trajectory can be slightly different if the heights of the magnetic sensors (i.e., their altitude from the floor) are different, but this difference is not substantial (see [5]).

Second, even the same magnetic sensors may exhibit different readings owing to a possible bias associated with their ferromagnetic materials, which depends on the history of magnetic readings. Figure 2.2(a) shows the magnetic sensor readings for the same magnetic sensor, at different distances from a ferromagnetic material (i.e., a battery). It shows the patterns of B_v along the same corridor as the distance varies between the sensor and the ferromagnetic material (1, 2, and 3 cm). The absolute difference increases as the magnetic disturbance increases, but again, the trends of signal change are similar (compare with Figure 2.1(b)). Thus, the signal differences owing to this bias can also be removed by applying the mean removal technique, as shown in Figure 2.2(b). Note that we also adopted here the ellipsoid-fitting calibration method [46] that can compensate the bias itself with a simple swinging gesture.

Third, for the same trajectory, different walking speeds of different users will result in different rates of changes in magnetic readings. Figure 2.3 shows the magnetic fingerprints of users moving at different speeds along the same trajectory. The rates of change in the magnetic data are different while the patterns

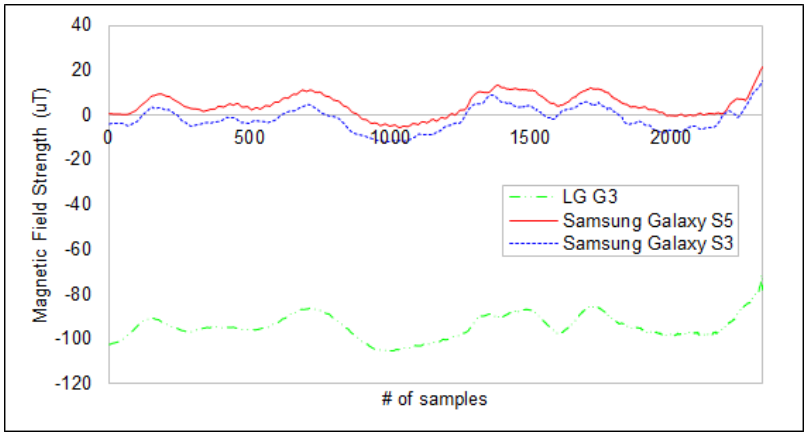

(a) before mean removal

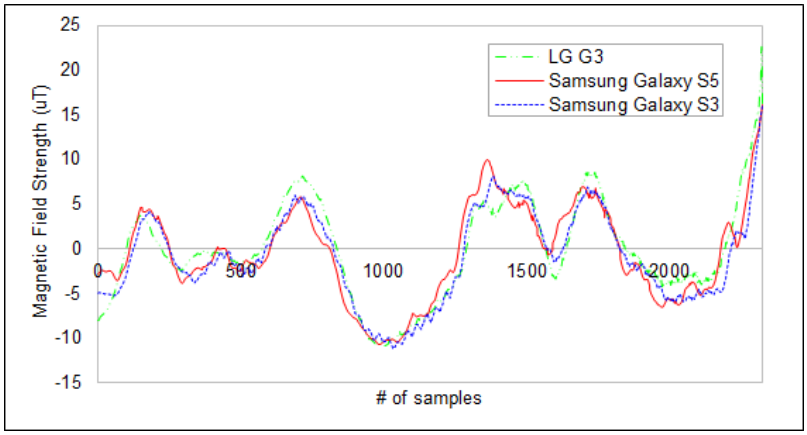

(b) after mean removal

Figure 2.1 Sensor readings from different magnetic sensors are plotted before and after mean removal, which shows that the relative change in magnetic readings along the trajectory is independent of magnetic sensors.

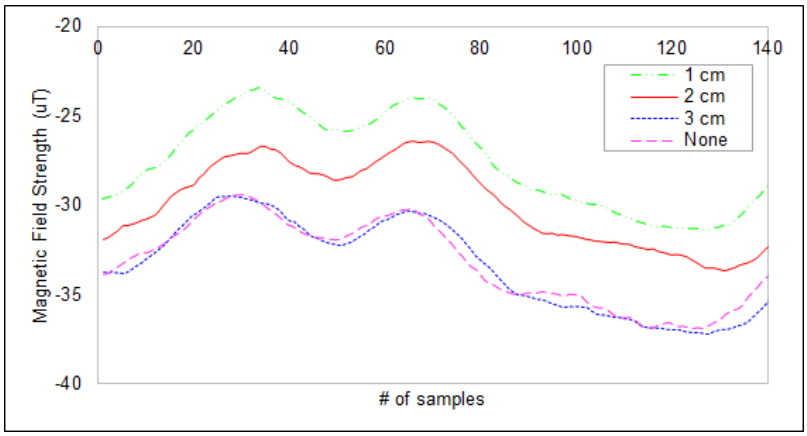

(a) before mean removal

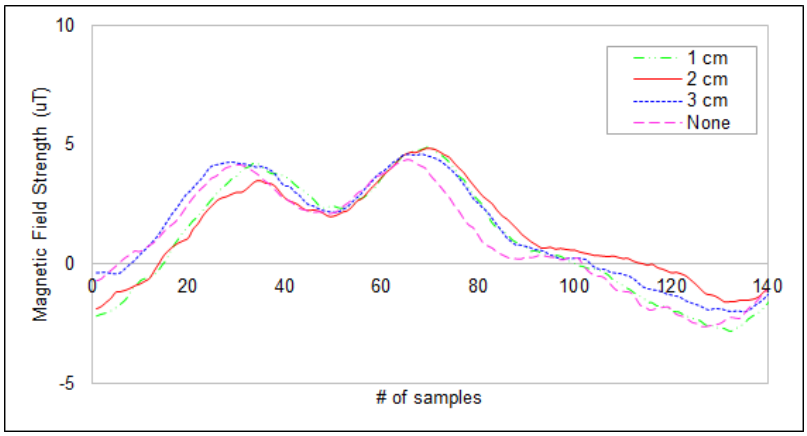

(b) after mean removal

Figure 2.2 Sensor readings from the same magnetic sensor are plotted before and after the mean removal, as the distance from the ferromagnetic material varies.

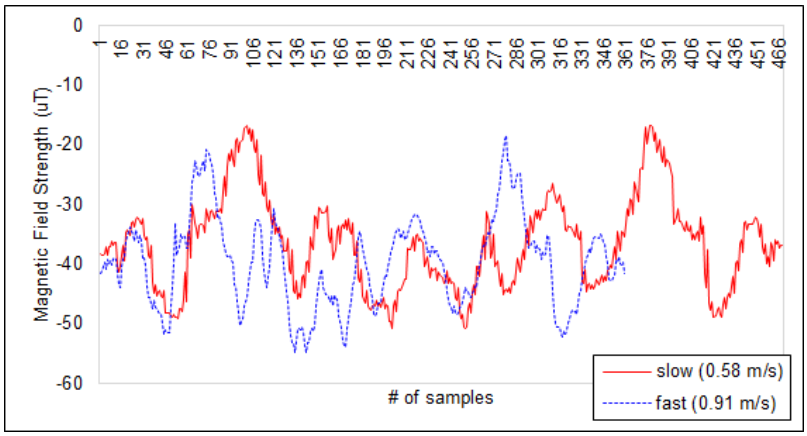

Figure 2.3 Sensor readings for users moving at different speeds.

of signals in the two plots are similar. This phenomenon may make the location finding/matching process somewhat more difficult. To address this issue, [6] leveraged the DTW algorithm [34]. The DTW algorithm allows to compare two sequences with different time scales or speeds. However, its complexity is so high that using the particle filter framework may demand many more system resources. Thus, in our approach we aimed to avoid using the DTW algorithm.

2.3.3 Sensing Rate

The rate of reading of a magnetic sensor is directly related to the amount of data to process. It decides not only how frequently the magnetic field data are acquired, but also how much of the device's energy is consumed. Thus, choosing the right sensing rate is important, especially considering the IoT paradigm. Recent smartphones can choose the sensing frequency in the range from dozens to hundreds Hz. As we seek to reduce the devices' energy consumption, we set the sensing rate to be as small as possible. Figure 2.4 shows the magnetic fingerprints for different sensing rates, for users walking at normal speeds. Compared

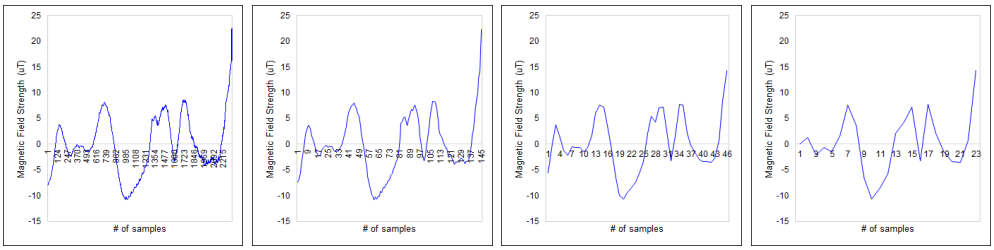

(a) 50Hz (b) 3Hz (c) 1Hz (d) 0.5Hz

Figure 2.4 Magnetic fingerprints obtained in the same corridor, for different sensing rates. Sensing rates as low as 3 Hz yield only marginal information loss.

with the fingerprint pattern for the 50 Hz sensing rate in Figure 2.4(a), the pattern for the 3 Hz sensing rate in Figure 2.4(b) exhibits almost no loss. Note that the fingerprint for the 1 Hz sampling rate in Figure 2.4(c) reveals some pattern losses, especially at the beginning and the end of the trajectory. We also plot the fingerprint for the 0.5 Hz sampling rate in Figure 2.4(d), which shows many pattern losses overall. We thus chose 3 Hz as the sensing rate.

2.4 Design of Energy-efficient Device for Localization

Considering the observations and issues, we now introduce the design of an IoT device for magnetic field-based localization.

2.4.1 Hardware Design

We aim to build a positioning system that uses IoT devices in office areas, in cooperation with SK Telecom, a leading mobile operator in South Korea. Among candidate platforms for IoT devices, we chose a small ID card, to which positioning functionalities were added. Figure 2.5 shows an ID card (right) in the size of a credit card, and a sensor-equipped board (left), in which the positioning functionalities were implemented. The width and the height of the

Figure 2.5 The implemented localization IoT device, in the form of an ID card on which a small board is mounted. The board contains a magnetometer, an accelerometer, and a BLE interface.

board were 23 mm and 52 mm, respectively, for mounting on the ID card.

The top requirement for the hardware design is energy efficiency, because we seek to achieve one-year lifetime for a coin battery system. We included only two sensors for localization: a magnetometer and an accelerometer. An accelerometer is essential for (i) the transformation from B_{raw} to B_{hv}, (ii) the PDR technique, and (iii) inferring the user's orientation. Other sensors, such as a gyroscope sensor and a barometer, can help enhance the localization performance; however, they were excluded from the present design, to reduce the device's energy consumption. We chose a KMX62-1031[55] sensor, which is an ASIC that consists of a 3-axis magnetometer and a 3-axis accelerometer.

For wireless communications, we chose a BLE chip [53] owing to its energy efficiency [47]. The BLE chipset used on the board was nRF52832 [56]. To localize the card's user in real time, the card/device continuously broadcasts a BLE advertisement frame that contains its sensor data. Thus, tuning advertisement-related parameters, such as the Tx interval and the Tx power,

Distance (m)	Observation Count	Transmission Count	Observation Probability
1	57	57	1.00
3	79	79	1.00
5	57	57	1.00
7	59	59	1.00
10	70	80	0.88
15	63	73	0.86

Table 2.1 The observation probability of BLE beacons vs. distance, for the Tx power of -20 dBm.

is a necessary step toward achieving energy efficiency. We set one second to be the Tx interval and -20 dBm to be the Tx power, to achieve the battery lifetime of one year, which was demonstrated in preliminary experiments. In the case of the Tx interval, one second is sufficient for tracking the position of the device's user. However, -20 dBm for the Tx power might be too weak for detecting at a certain distance, which required us to conduct the following experiments.

Table 2.1 shows the observation probability of the BLE beacon frames vs. the distance between the BLE access point (AP) and the Tx device, with the Tx power set to -20 dBm. The observation probability decreases for distances longer than 10 m. In our experimental environment, four BLE APs were deployed at every corner of a square-shaped office area in a grid format, and the length of a side of a square was 20 m. The case in which every AP received no beacon frames consecutively occurred infrequently during the entire evaluation process, owing to many APs. To make up for missing a single beacon frame, the device also sends the magnetic field data of the previous round.

2.4.2 Structure of the BLE Beacon Frame

Figure 2.6 shows the message format of the BLE advertisement frame, which is used for conveying the sensory data from an IoT device to a localization server in our system. The maximal size of the BLE advertisement frame is currently 31 bytes according to [53]. In the proposed system, the available space for the sensory data is 19 bytes, since 12 bytes are reserved for other data, including the company ID, the device's status, the remaining battery level, and the sequence number. We first contain a series of three pairs B_h and B_v in the current round (1 round = 1 s), where each value is 2 bytes long. Recall that the sensing rate is 3 Hz. Note that each value ranges from -1200 uT to +1200 uT [55]. Thus, the total number of bytes for reading magnetic vectors is 12. Then, the series of three $|B|$ values of the previous round needs 3 bytes; this is to make up for beacon missing cases, as mentioned in Section 2.4.1. Even though a single value ($|B|$) may make it difficult to distinguish the magnetic fingerprint of one location from others, we cannot afford to keep two values (B_h and B_v) for the previous round, due to the space limit. In the case of the accelerometer, its sensing rate is 6 Hz, and each reading needs 0.5 bytes for its vector strength. Overall, that requires $6 * 0.5 = 3$. The acceleration data itself are used only in the step detection, and the detection algorithm does not require high-resolution data, as will be detailed in Section 2.5.3. The last byte is assigned to the average value of the orientation observed in the current round. The change of the user's heading direction in the indoor space tends to be not so frequent. Thus, a single orientation value per second is sufficient to track the direction of the user's movement.

Item	*Metadata* *(seq. #, battery, status, …)*	B_v	B_h	*last* |*B*|	|*acc*|	*Orientation*
Bytes	12	6 (3 * 2 bytes)	6 (3 * 2 bytes)	3 (3 * 1 bytes)	3 (6 * 0.5 bytes)	1

Figure 2.6 A BLE beacon frame contains the magnetic data, accelerometer data, and orientation data.

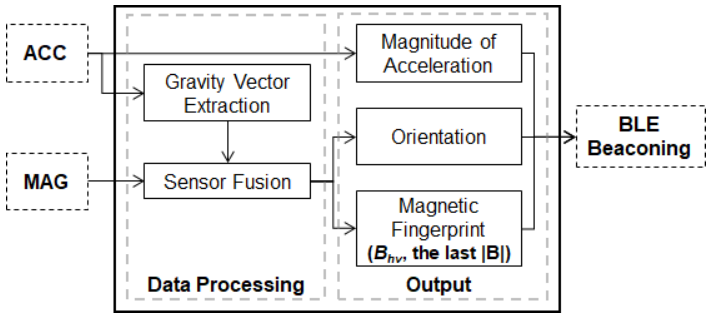

Figure 2.7 The building blocks of the proposed indoor positioning device: a magnetometer, an accelerometer, and a BLE interface.

2.4.3 Processing Sensor Data

In the proposed system, the device delivers the sensor readings to a back-end server via BLE APs. In this way, device-end data processing is minimized for energy saving purposes. However, owing to the space limitation of the BLE advertisement frame, front-end processing of sensory data should be performed in the device to compress the data that are to be delivered. Figure 2.7 shows the device architecture including data processing components and their inputs/outputs. Calculating $|acc|$, transforming a three-dimensional magnetic vector to a two-dimensional value (denoted by B_{hv}) [27], and averaging the orientation values [11] are straightforward.

As to extracting the gravity vector from the raw accelerator vector, many papers [49, 50, 51] have used an N-order Butterworth low pass filter (LPF) [48].

However, despite its good filtering performance, the Butterworth filter has $O(N \log N)$ the temporal complexity [52] of the fast Fourier transform (FFT). Thus, it requires too much computational power and memory for IoT settings. We note that the main purpose of extracting the gravity vector is to obtain B_{hv} by rotating B_{raw} onto the gravity plane. For lightweight operations, we replaced the Butterworth filter by a first-order LPF as follows, since a simple LPF can calculate B_{hv} approximately

$$y_i = a * x_i + (1 - a) * y_{i-1} \tag{2.1}$$

where x_i is an input value at the current time, and y_i, y_{i-1} are output values at the current time and previous time, respectively. Here, a is a constant for the LPF.

Equation (2.1) is a simplified formula for the first-order LPF. This LPF is much simpler than the Butterworth filter and requires memory only for a single floating number y_{i-1}. To evaluate the performance of filters, we first recorded the acceleration data and B_{raw} for subjects walking along the corridor, and rotated the B_{raw} vector by different gravity vectors extracted using different filters. A gravity vector obtained using a commercial gravity sensor of Samsung Galaxy S5 and a magnetic fingerprint rotated by raw acceleration were also used for comparison. Figure 2.8 plots only B_v, which shows that the patterns of magnetic fingerprints are almost similar. We thus used the simple first-order LPF in Equation (2.1).

As the final validation process, we compared the magnetic fingerprints obtained by a smartphone and the presently designed IoT device. The two fingerprints exhibited almost the same pattern along a 150-m-long trajectory in terms of B_h and B_v, respectively, as shown in Figure 2.9.

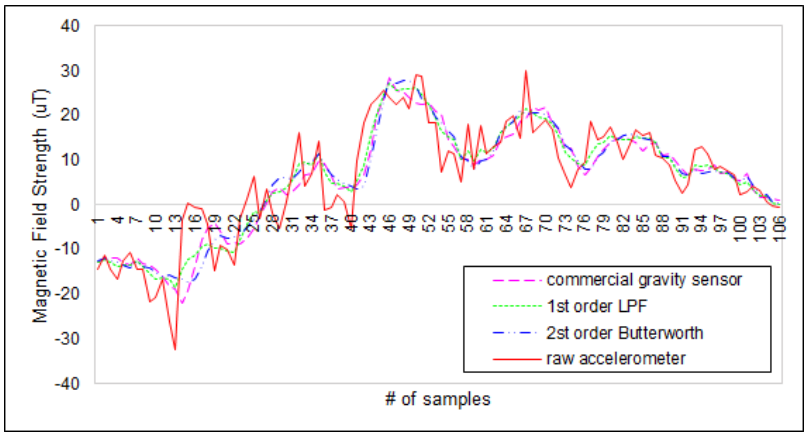

Figure 2.8 Magnetic fingerprints extracted using different gravity vectors, for the same path.

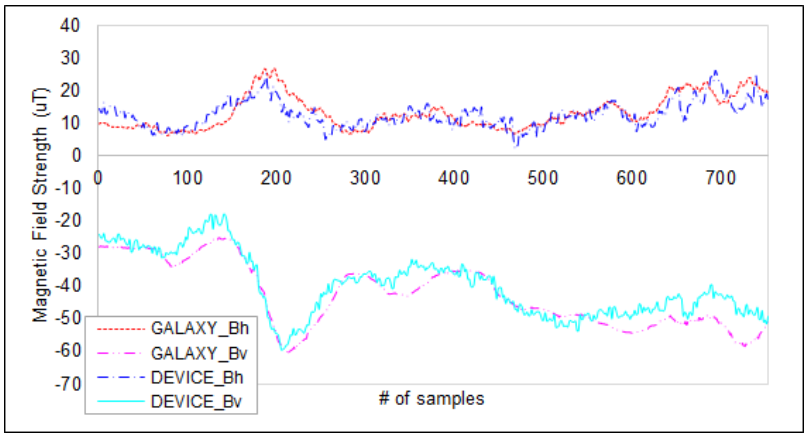

Figure 2.9 Magnetic fingerprints obtained from a smartphone and the designed IoT device, for the same path.

2.5 System Architecture

We now introduce the architecture of the proposed system and the positioning algorithm, whose designs are based on the findings described in the previous sections.

2.5.1 Overview

In the proposed system, the positioning algorithm starts when a user carrying a neck ID card enters the target area. The card/device periodically advertises a BLE beacon frame with sensor readings as specified in Figure 2.6. The BLE APs positioned in a grid-like manner (intervals of 20 m) then receive the frame, which in turn is delivered to a back-end server. The APs each collect the received signal strength (RSS) of the received beacon frame for localization purposes. We analyze the BLE RSS along with the magnetic field data, to enhance the localization performance.

After receiving the beacon frames, the back-end server estimates the location of the user, using the particle filter algorithm. The computation is performed for each period (period duration, 1 s). The server first counts the number of footsteps and moves the particles depending on the step count and the orientation. Then, the user's final location is estimated using the particle filtering process, which will be described in details below.

2.5.2 Site Survey Methodology

For the site survey, we used the same magnetic fingerprint collection method as in Maloc [5]. In Maloc [5], the surveyor collected (and interpolated) magnetic fingerprints at every 0.1m * 0.1m grid points by moving in the target area along straight-line paths. However, storing fingerprints with such a fine

granularity leads to a huge fingerprint database and high computational cost. What is worse, as the number of measurement points increases, there are likely to be more points with the same or similar magnetic reading. To determine the suitable size of a grid unit, we divided a 2-m-wide corridor into seven straight-line paths with 0.3 m intervals, which were numbered from 1 to 7, from the left to the right direction. Figure 2.10 shows the magnetic fingerprints along the different paths. We found that two adjacent fingerprints exhibited similar patterns, while next-nearest fingerprints tended to exhibit distinct patterns. Moreover, using the insights in 2.3.3, we also estimated the proper grid size by observing the magnetic data along the same path. That is, the spatial change in the magnetic field data along a path was marginal for a certain distance. If the sensing rate of 3 Hz is sufficient for tracking the magnetic fingerprint pattern of a user when the user walks at a normal speed ranging from 1 m/s to 1.5 m/s, we can obtain only one or two fingerprint data for each 0.5 m unit as a representative value. We thus chose 0.5 m as the grid size based on the above findings.

We implemented an Android application for convenient site surveying, and Figure 2.11 shows a screenshot of this application. The surveyor can easily choose the target grid for measurements. We also incorporated a PDR module into the application, hence allowing to map collected fingerprints to proper grids, even if the surveyor walks at various speeds. Note that we use the average values of B_h, B_v, and the RSSs received by the BLE APs nearby as the fingerprint of each grid.

2.5.3 Particle Filter Framework

In this section, we explain the particle filter framework that is used in the proposed system. The particle filter solves the filtering problem, which amounts

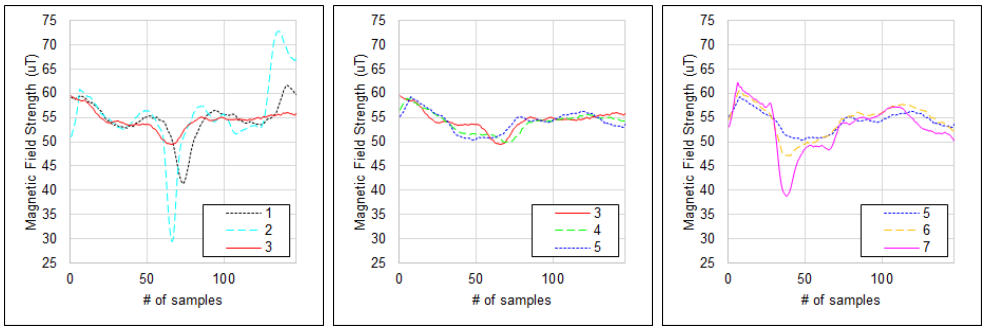

(a) Left-side paths (b) Middle paths (c) Right-side paths

Figure 2.10 Fingerprints collected along multiple paths (in a corridor), with the distance of 0.3 m between adjacent collection sites.

to estimating the state of a dynamical system (i.e., the location of a user) from noisy and partial observations. The key action of the particle filter consists of distributing a set of particles (also called samples) in each epoch, to represent the probability distribution of the state of the dynamical system. In the next epoch, the observation is different, owing to the dynamical nature of the system, which is manifested as replacement of old particles (of negligible probabilities) by new particles or moving particles into a new distribution.

Step Counting

First, we should count the number of steps for moving the particles. In our system, there are only six $|acc|$ values per second owing to the space limitation on the beacon frame; thus, we use a simplified heuristic algorithm for counting the number of steps. We adopted the peak-valley detection technique [4, 25], which allows to count the steps using a simple algorithm. It is widely known that the temporal change in the acceleration (of a walking user) exhibits a periodic pattern of alternating peaks and valleys. Thus, steps can be counted

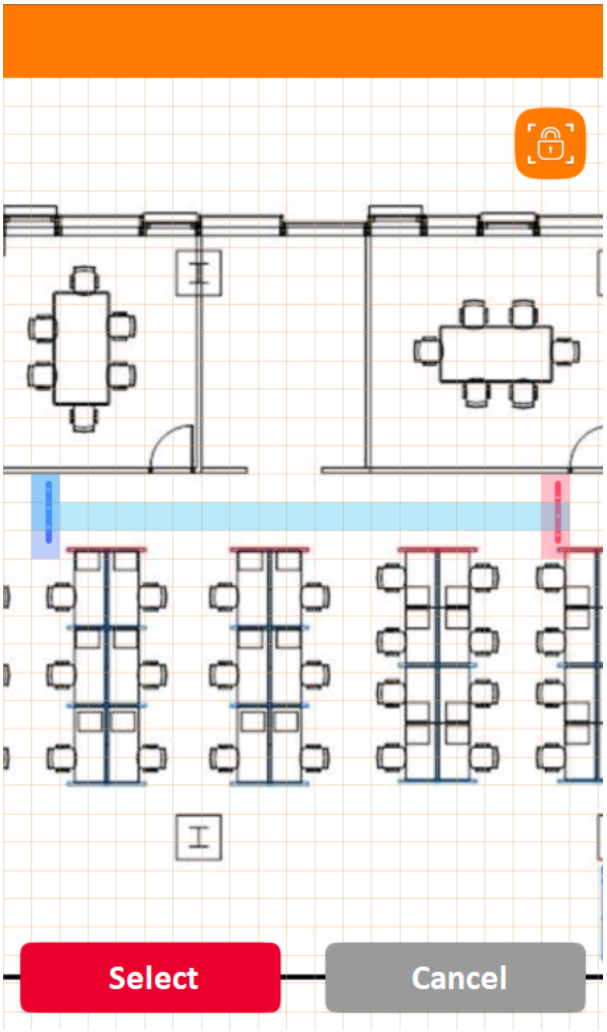

Figure 2.11 A screenshot of the site survey app, captured to illustrate the convenience of fingerprint measurements.

by tracing this pattern.

In our approach, we collect the acceleration magnitude (i.e., raw floating data) as the user walks 15 steps with the sampling frequency of 15 Hz, as shown in Figure 2.12(a), and the measurements are filtered by the proposed system (6 Hz, rounded off to integers), as shown in Figure 2.12(b). To clearly trace the peaks and valleys in our measurements, we designed the device firmware to compute the maxima and minima of the acceleration magnitude three times during a time window (1-s-long window). Thus, three max-min pairs (of the acceleration magnitude data) for each time window are transmitted over the BLE interface. Obviously, some information is lost owing to compression, but the data critical for the peak-valley detection technique are delivered. Next, we determine the peaks and valleys in the sequence by applying two thresholds: $12m/s^2$ for the peaks and $8m/s^2$ for the valleys. We also consider the increasing and decreasing trends in the overall sequence for excluding false peaks and valleys. The red dots in Figure 2.12(b) show the results obtained using our step-counting algorithm. The accuracy of the step-counting algorithm over the entire evaluation process was above 90%.

Motion Model

Although the distortion in the magnetic field in an indoor environment can be used as a fingerprint, it also hinders us from inferring the heading orientation of a user/device. This phenomenon directly and negatively affects the performance of the particle filter technique, because particles should move in the same direction as the user's orientation. To overcome this problem, we adopted a technique that was introduced in Magicol [6]. Magicol exploits the observation that a walking human is very likely to follow the direction of a corridor, rather than making random turns. However, we have to propose an alternative

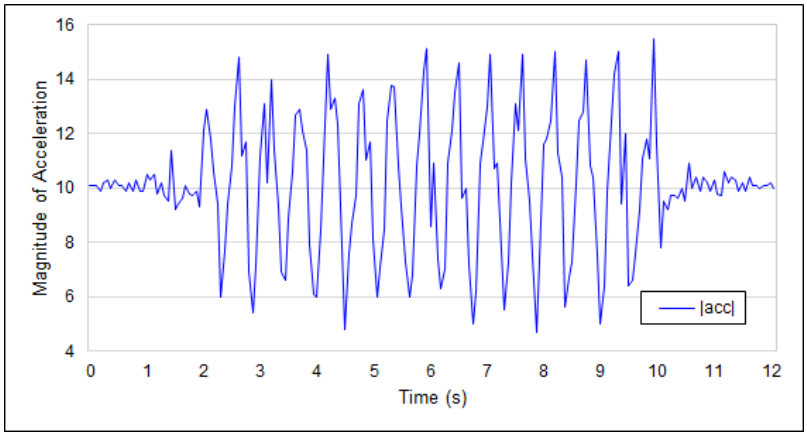

(a) raw acceleration data (15Hz)

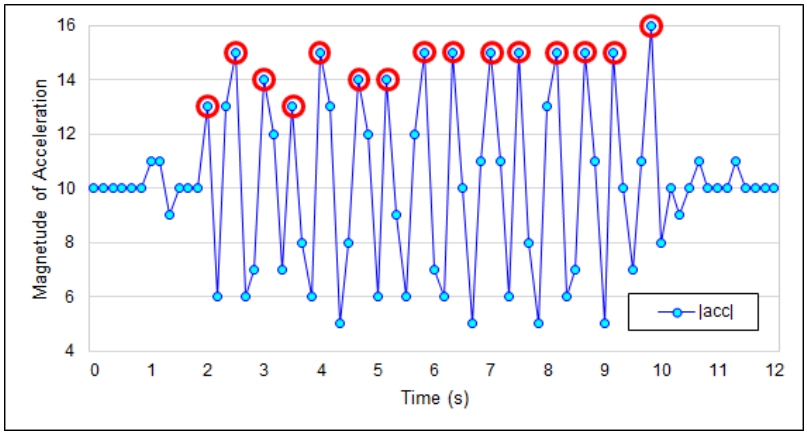

(b) acceleration data from our device (6Hz) and step counting result

Figure 2.12 The temporal pattern of the acceleration magnitude and the result obtained using the proposed step-counting algorithm, for a user walking 15 steps.

solution because we cannot use a gyroscope sensor (to track the user's heading more correctly) as in Magicol.

To ensure that particles follow the user's walking direction, we take a probabilistic approach substantiated in Algorithm 1. Forty percent of the particles move along the pathway (one out of several candidate pathways) whose direction is closest to the orientation reading of the device. Another 40% of the particles choose a direction by considering the extrapolation of the user's movement between the previous and current rounds. The remaining 20% of the particles move simply following the raw orientation reading (regardless of the pathway). The proposed model is thus likely to force most of the particles (˜80%) move along the (estimated) pathway direction. Figure 2.13 shows that this algorithm (indicated by Motion Model) traces the user's walking orientation with the accuracy of 84%, even if the user makes 11 turns on the trajectory. Here, GT denotes the ground truth direction of the user. Note that the magnetic reading for the orientation can be far from the real direction of the user, owing to distortion.

While other magnetic field-based systems, such as Maloc [5] and Magicol [6], aggressively leverage the accurate estimation of orientation using a gyroscope, the proposed motion model achieves high accuracy in spite of the much lower sensor rate (1 Hz) and the absence of a gyroscope. Our probabilistic approach that tracks both the pathway's direction and the history of the user's trace effectively estimates the user's true orientation in structured indoor environments. The performance of the motion model directly affects the posterior distribution of states in the particle filtering framework.

Magnetic Matching

After all particles move, the survival probabilities (weights) of the particles

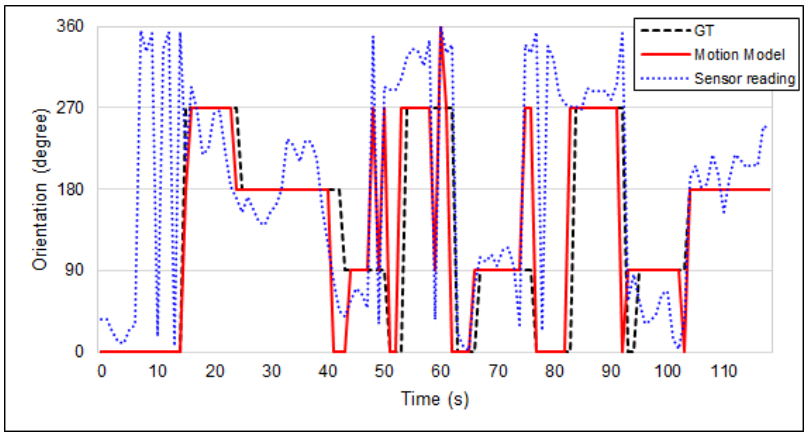

Figure 2.13 Performance of the motion model algorithm for inferencing the user's orientation. Raw orientation readings were obtained and calibrated by the motion model that achieved 84% accuracy on a trajectory with 11 turns.

need to be computed. As described in 2.3.1, the weight of a particle is computed using the temporal history of B_{hv} as a fingerprint to overcome the low distinctiveness of magnetic field data. Prior approaches [2, 6] that used magnetic field history data exploited the DTW algorithm to compare the similarity between magnetic fingerprints to support various walking speeds. However, the DTW technique is expensive both computationally and memory-wise, especially when used with the particle filter framework that computes the weight of every particle. Thus, in our approach we exploit the Euclidean distance to lower the computational complexity when comparing the similarity between the observed fingerprint and patterns in the database.

To exploit the Euclidean distance to find the matching entry in the database, the speed of the user's fingerprint measurements should be estimated first. As explained in Section 2.3, various walking speeds and sensing rates of the device along the same path may generate seemingly different fingerprint patterns. As

the sensing rate is fixed at 3 Hz in the proposed system, the issue that remains to be resolved pertains to different walking speeds of the user and the (site) surveyor. We resolve this issue by (1) allocating a wide range of stride lengths for each particle, and (2) disseminating the particles in a wider area in the proposed particle filter framework during the resampling of dead particles. With the sensing rate fixed, the differences between the fingerprint patterns of different users are relatively small. Thus, moving the particles to some area including the true location of the user is easily achieved using the two above-mentioned techniques. Although we should use many particles (about 3000) to cover the wide range of stride lengths and hence the wide area of dissemination during the resampling, the increase in the execution time with the Euclidean distance is much smaller than the one for the DTW technique (detailed in Section 2.6).

BLE Matching

In our approach, we also used the BLE matching technique as a supplement to the particle filter framework. We first adopted a traditional fingerprinting approach introduced in RADAR [1] for BLE matching. In the fingerprint database, each grid of the target area contains a BLE RSS fingerprint obtained during the site survey, which allowed us to infer the best-matched grid by comparing the user's BLE RSS observation and the database content. However, owing to the weak intensity of BLE signals compared with WiFi, the localization performance of BLE fingerprinting may be somewhat unstable. Thus, augmenting the BLE matching results with particle weighting does not improve the overall performance of the system.

When we extend the magnetic field data in the time domain for fingerprinting, we should decide how many readings of the magnetic field data will be sufficient for achieving the desired localization performance. To this end, we

conducted a pilot experiment to decide the time duration that is necessary to make the temporal history of magnetic readings distinct; it took about 10 s (10 m to 15 m in the moving distance) for a sequence of magnetic data to acquire distinct history. Hence, we used the BLE matching combined with the magnetic fingerprint to improve the overall localization performance. For the first 10 s after the initialization, we remove the particles that are beyond a certain range R_{BLE} from the BLE matched grid. Note that the particles around the GT point should not be removed. For that, we count how many times a particle is outside the R_{BLE} range consecutively; if the particle is outside for the duration τ_c, it is removed. We call this technique *BLE filtering*. Also, we set τ_c to 2 and R_{BLE} to 6 m to speed up the convergence of the particle distribution.

Particle Filter

We now combine the above component processes into a particle filter framework. Equation 2.2 shows the particle model for particle p_i in the proposed system

$$p_i =< x_i, y_i, \theta_i^{t-1}, w_i, c_i, \vec{h} > \tag{2.2}$$

where x_i, y_i represent the current location of particle p_i, which captures the candidate user location. The parameter θ_i^{t-1} is the orientation measure in the previous round (i.e., $t-1$) and w_i represents the weight of the particle. The quantities c_i and $\vec{h}$ denote the *BLE filtering* count of the particle and the temporal history of B_{hv} that the particle has observed along its trajectory, respectively.

During the initialization phase, the particles are uniformly distributed throughout the target area. Then, for each beacon, the position and the weight are updated. At first, the position of particle p_i at time t is updated based on the

step-counting and motion model algorithms, using Equation 2.3

$$(x_i^t, y_i^t) = \begin{cases} x_i^t = x_i^{t-1} + N_{step}^t \times (l + G_l) \times \cos(\theta_{mm}^t + G_\theta) \\ y_i^t = y_i^{t-1} + N_{step}^t \times (l + G_l) \times \sin(\theta_{mm}^t + G_\theta) \end{cases} \tag{2.3}$$

where N_{step}^t is a detected step count at time t, l is 0.65 m as a mean value of the stride length distribution, and θ_{mm}^t represents the calibrated orientation obtained using the motion model. G_l and G_θ are Gaussian noise processes of the stride length and orientation, respectively.

We add a relatively higher Gaussian noise to the stride length as $G_l \sim \mathcal{N}(0, 0.5l)$ compared with the existing approaches (e.g., $\sigma = 0.2l$ as used in [6]), to expand the distribution area of the particles to support various walking speeds (of users). The Gaussian noise for the orientation is set to $G_\theta \sim \mathcal{N}(0, 10^\circ)$.

After the particles move, their weights should be updated. In our approach, we adopted a Gaussian weight function, following [6]. The Gaussian function effectively enhances the distinctiveness of the magnetic fingerprint patterns owing to its bell-like shape. Equation 2.4 describes the weight function

$$w_i = \alpha e^{-\frac{\|d\|^2}{2\sigma^2}} \tag{2.4}$$

where α is the height of the Gaussian curve's peak and the maximal value of the magnetic weight, σ is the aggressive parameter to control the width of the Gaussian curve, which captures how aggressively the weight decreases as $\|d\|$ increases. Here, $\|d\|$ is the Euclidean distance, as shown in Equation 2.5

$$\|d\| = d(\vec{h}, \vec{u}) \tag{2.5}$$

where $\vec{u}$ is the vector of B_{hv} measured by the device.

Note that the mean removal technique is applied to $\vec{h}$ and $\vec{u}$, respectively, as explained in Section 2.3.2. After updating the particle's weight, the particle is removed if it satisfies any of the following conditions.

1. The particle hits the wall
2. w_i is lower than a threshold τ_w
3. BLE filtering

The final phase of the particle filter algorithm is resampling and the inference of the user's location. As explained in 2.5.3, we adopt here a heuristic algorithm to maintain a sizable area for particle dissemination to support various walking speeds of users. For the removed particles, we replenish the same number of new particles around the survived particles with top 10% of weights. At this moment, the distance between surviving and replenished particles is randomly distributed within a circular area of its radius being 1.5 m. Finally, to infer the final location of the user, we calculate the average of the coordinates over all of the particles, weighted by w_i.

2.6 Evaluation

In this section, we evaluate the proposed system in terms of the localization accuracy, computational cost, as well as energy efficiency. The evaluation consists of (1) parameter tuning for the particle filter algorithm such as the temporal sequence of $\vec{h}$ and number of particles P, (2) comparing the effectiveness of the Euclidean distance (EUC) approach with the DTW approach, and (3) measurements of battery consumption for the prototype device.

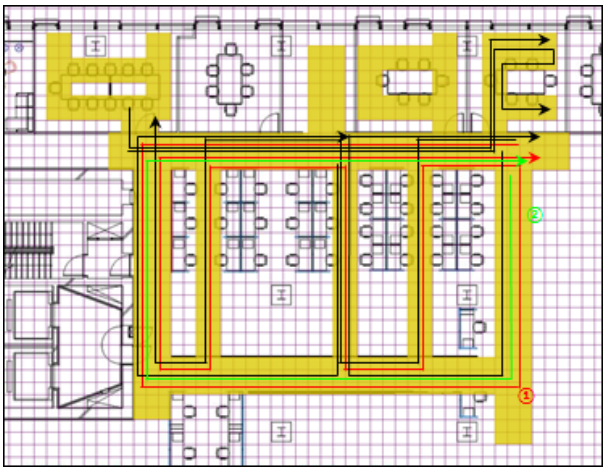

Figure 2.14 Evaluation of the proposed system in a 20.5 m × 16 m office area with three conference rooms.

2.6.1 Implementation

We first implemented an IoT device for localization, as shown in Figure 2.5, and its firmware as described in Section 2.4. When the testers carrying the device walked in the target area, the device continuously delivered sensor readings to the back-end server via the BLE APs. Note that the four BLE APs were organized in a grid-like manner (with 20 m intervals) at the four corners of the testbed. Then, the particle filter framework implemented on the back-end server PC with a 3.3 GHz CPU and 16 GB memory estimated the location of the device based on the sensor readings. The particle filter framework could perform both real-time and off-line analysis after collecting user traces. We chose the latter to evaluate the proposed system against the ground truth for the sake of simplicity.

2.6.2 Experiment Setup

To evaluate the performance of the proposed system in a real-world setting, we collected sensory data in a 20.5 m $\times$ 16 m office area, as shown in Figure 2.14. The target area contained three conference rooms and multiple corridors. To support the various moving speeds and stride lengths of target users, three testers with different heights collected the data for three months, from February to April of 2017. We defined seven trajectories in the target area, among which two trajectories each were tested at three speeds (0.58 m/s, 0.91 m/s, and 1.30 m/s) and three device heights (0.9 m, 1.1 m, and 1.3 m). The other five trajectories were tested for speeds in the 1.0 - 1.1 m/s range. In Figure 2.14, two trajectories are drawn in red and light green, and the others are drawn in black. Using the collected data, we evaluated the system in terms of the localization accuracy, computational cost, and energy efficiency.

2.6.3 Localization Performance

Temporal Duration of Magnetic Readings

We first evaluated how the temporal duration of the magnetic readings (i.e., $\vec{h}$) affected the localization performance in Figure 2.15. Figure 2.15(a) compares the localization accuracy of the Euclidean distance (EUC) and the DTW algorithms, for different temporal duration of $\vec{h}$. Note that we assigned 3000 particles in this experiment. Figure 2.15(a) shows that both algorithms achieved the accuracy of 2 m when we set the temporal duration of $\vec{h}$ to be longer than 20 s. The execution times for the EUC and DTW methods, plotted in Figure 2.15(b), show that the difference between the EUC and DTW methods increases significantly with increasing temporal duration of $\vec{h}$. Interestingly, the execution time of the EUC algorithm appears to converge, even when the

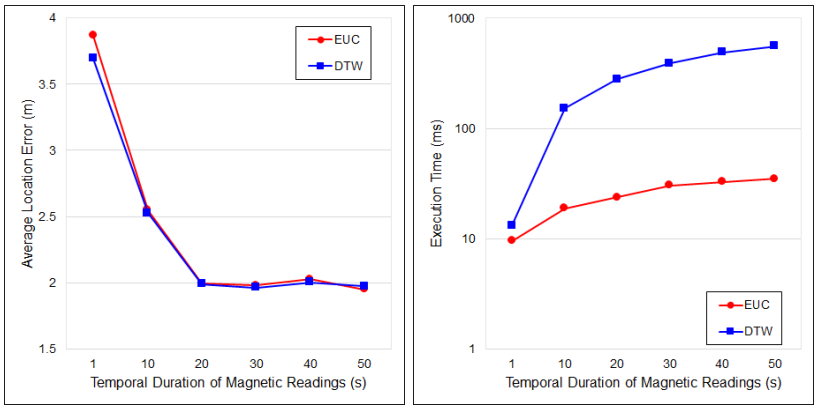

(a) Localization performance (b) Execution time

Figure 2.15 Effect of the temporal duration of magnetic readings on the localization performance and on the execution time.

temporal duration of $\vec{h}$ increases. Hence, we conservatively chose 30 s as the temporal duration of magnetic readings (i.e., 90 samples) in what follows.

Number of Particles

The number of particles, P, in the particle filter algorithm is a key parameter directly linked to the localization performance and the computational cost. Figure 2.16 shows the time-series localization performance when a target user walks along the trajectory ① as shown in Figure 2.14. We assigned two numbers to P: 500 (Figure 2.16(a)) and 3000 (Figure 2.16(b)).

With $P = 500$, as shown in Figure 2.16(a), the EUC method poorly traces the movement of the target user when two turns are made with a short interval (around 75 and 79 s). It then spends almost 30 s on catching up with the target user at the similar localization accuracy as the DTW method. The main reason for the poor performance of the EUC method with $P = 500$ is that a wide but sparse distribution of particles may not cover the ground-truth location

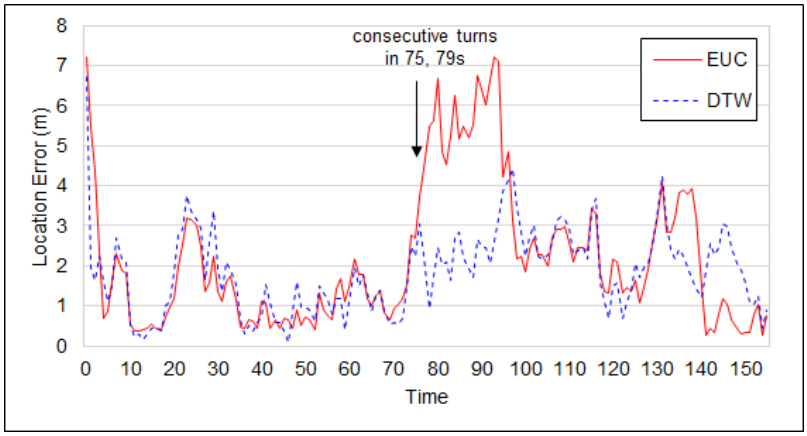

(a) $P = 500$

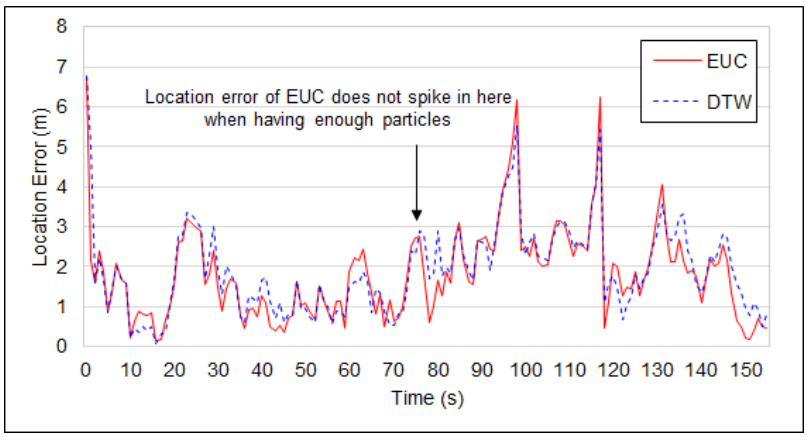

(b) $P = 3000$

Figure 2.16 Localization performance of the EUC and DTW methods, for different numbers of particles in a long trajectory.

of a target user. On the other hand, in the case of $P = 3000$, as shown in Figure 2.16(b), the localization errors for the EUC method around 75 s and 79 s do not spike owing to the sufficient density of particles. Interestingly, the EUC method with $P = 3000$ performs even better than the DTW method with the same number of particles. That is, the average localization error of the DTW method is 1.92 m, while that of the EUC method is 1.81 m. All of the experiments for all scenarios demonstrated the same tendency, as shown in Figure 2.19(a). As shown in Figure 2.19(a), using the DTW method with $P = 500$ ($DTW500$) was slightly advantageous to using the EUC method with $P = 500$ ($EUC500$), but the performance gap between the $DTW3000$ and $EUC3000$ methods was negligible, owing to the sufficient number of particles.

We also evaluated the effect of the heuristic algorithms (in Section 2.5.3) that can contain the candidate locations (by placing the particles as explained in Section 2.5.3) when they run with the sufficient number of particles, $P = 3000$. Figure 2.17 compares the results for $EUC3000$, with and without these heuristic algorithms. As shown in Figure 2.17, the performance of the EUC method without these heuristic algorithms is significantly compromised, which implies that these heuristic algorithms are effective when a sufficient number of particles is used.

We next compared the computational cost of the EUC and DTW methods, and the results are shown in Figure 2.18. Figure 2.18 shows the computation time for a single-round particle filter algorithm. As shown in Figure 2.18, the EUC method is more computationally efficient. Since we set the temporal duration of $\vec{h}$ to 30 s, the accumulated history size of the DTW method gradually increases until 30 s from the start, and maintains the same size after that point. On the other hand, the execution time of the EUC method is almost the same up to 30 s from the start. Moreover, the EUC method yields a 15x faster

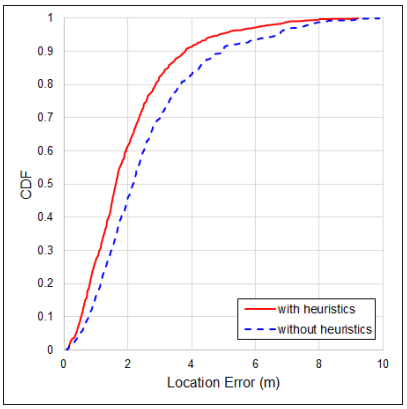

Figure 2.17 Effect of the heuristic algorithms in the augmented particle filter for a system with 3000 particles.

execution time than the DTW method on average (450 ms for DTW, 30 ms for EUC). This also holds for different scenarios with different P, as shown in Figure 2.19(b). Note that the execution time of $DTW500$ is even 2.7x times longer than that of $EUC3000$; the median execution time of $EUC3000$ is 29 ms, while that of $DTW500$ is 78 ms. Considering the comparable localization performance of $EUC3000$ and $DTW3000$, as shown in Figure 2.19(a), we conclude that leveraging the Euclidean distance can achieve a comparable localization performance to that of the DTW approach, while being more computationally efficient (and thus more energy efficient).

Finally, we set the number of particles to 3000 in the proposed system, i.e., $EUC3000$. Figure 2.19(a) shows the localization errors for the different algorithms. For comparison, we also evaluated the PDR-based particle filter algorithm (PDR_RAW) without the motion model and the BLE fingerprinting algorithm adopting RADAR [1] (BLE_RADAR). The average localization error of the proposed system for every scenario was 1.96 m, and the median error was 1.62 m. This result indicates that the proposed system performs almost

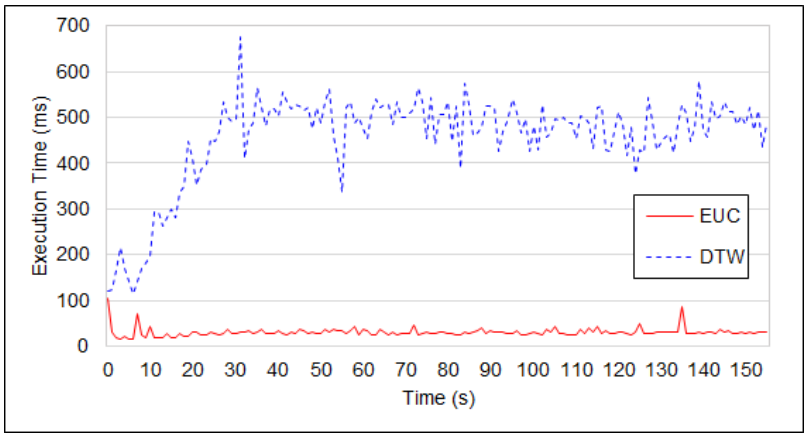

Figure 2.18 Comparison of execution times of the EUC and DTW methods, with $P = 3000$, for a long trajectory.

as well as systems that use smartphones [5, 6] and the DTW approach. At the same time, the proposed system is more computationally efficient than other systems, as shown in Figure 2.19(b). In comparison with Magicol [6] and Maloc [5] approaches, for which the execution times are longer than 3 s and 1 s, respectively, our system performs much faster owing to the smaller number of sensors and data rate, and because it does not use computationally heavy algorithms such as the DTW algorithm.

BLE Filtering

Figure 2.20 analyzes the efficiency associated with incorporating the *BLE filtering* technique into the particle filter framework. As shown in Figure 2.20(a), *BLE filtering* reduces the localization error and its convergence time, especially in the first part of the experiment. Figure 2.20(b) shows the cumulative distribution functions (CDFs) of the localization errors, for different scenarios. As shown in Figure 2.20(b), the localization performance is improved, especially

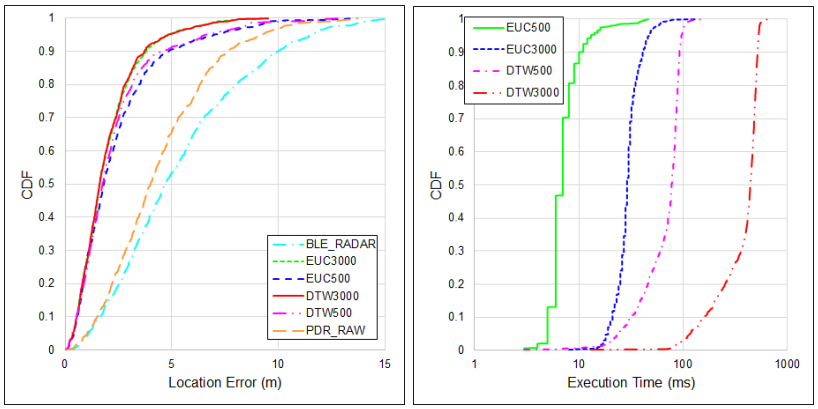

(a) Localization performance (b) Execution time

Figure 2.19 Localization performance and execution time for different algorithms, for different numbers of particles P.

for the cases with large localization errors, because *BLE filtering* reduces the convergence time.

2.6.4 Energy and Algorithmic Efficiency

We next evaluated the energy efficiency of the IoT device by measuring its energy consumption, and the results are shown in Figure 2.21. We observed that the device uses 0.159 mA in the active mode, during which it performs continuous BLE advertisements at 1 Hz, while it requires 0.004 mA in the sleep mode. The battery we used in the proposed device was a CR2450 [57] with the 620 mAh capacity. Hence, assuming the device is used 8 h a day, the device can be used for 324 days. Note that switching between the active and sleep modes can be easily triggered by sensing the magnitude of acceleration.

We also evaluated how many IoT devices a typical back-end server (i.e., with 2.2 GHz CPU and 16 GB memory) can handle. To this end, we implemented a benchmark software that emulated multiple devices in the proposed particle

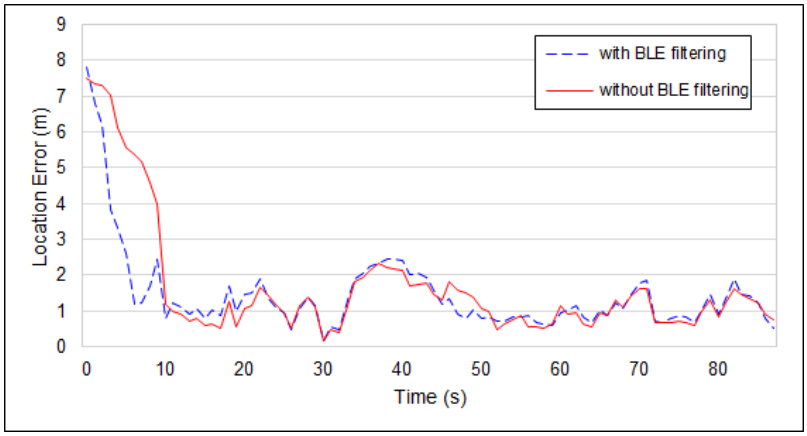

(a) The change in the localization performance as the user walks for 90 s

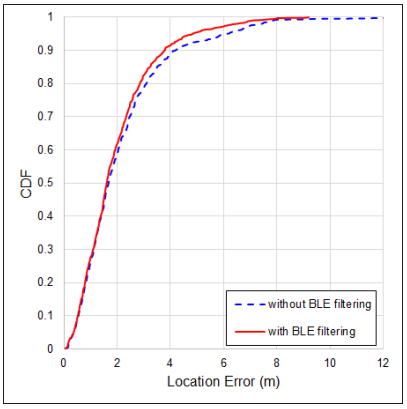

(b) CDFs of localization errors for all the experiments

Figure 2.20 Effect of the BLE filtering technique.

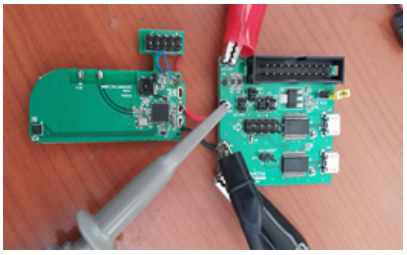

Figure 2.21 Energy consumption of the developed IoT device.

filter system. As shown in Table 2.2, the CPU usage (of the back-end server) increased with increasing the number of devices. We found that a desktop-level machine can handle about 60 devices. Therefore, we expect that the proposed system can simultaneously support hundreds of devices with a high-end server machine.

2.7 Discussion

Comparison with Other Indoor Localization Systems We compared our system with other representative indoor localization systems in Table 2.3. Methods that leverange WiFi signals, such as Horus [21], are the most widely used ones, owing to the wide deployment of WiFi APs. However, WiFi scanning takes 3-4 s, and also consumes much energy. UWB-based systems [37] achieve very high accuracy on the centimeter scale and provide real-time positioning services. However, they still suffer from the problems of high energy consumption [36] and high deployment cost, due to the need for customized hardware devices. From the viewpoints of both energy consumption and scanning frequency, systems that are based on BLE [35] can be a good alternative. However, they are characterized by a high cost for dense installation of BLE beacons. Moreover, frequent fluctuations of these wireless signals (including WiFi, BLE, UWB), caused by the multi-path effect and human body blockage, often make the localization performance of these systems unstable. As a way to overcome the inherent weaknesses of wireless signals, some studies [43, 44] have proposed visible light-based localization systems. These systems achieve very high positioning accuracy and their deployment cost is much lower, because there are already ubiquitously deployed fluorescent lights and light-emitting diodes (LEDs) in buildings. The drawbacks are (i) high energy consumption

associated with the camera operation and vision data analysis, and (ii) line-of-sight (LoS) path requirements on the light sources.

On the other hand, as explained in Section 2.3.1, the robustness and pervasiveness of magnetic fields make magnetic field-based systems more viable than systems based on other localization sources. The magnetic field is not affected by obstacles and is nearly stable in time, and its discernibility can be enhanced by using the temporal history of B_{hv} as a fingerprint. Compared with previous studies [5, 6], our system is more energy and algorithmically efficient. Our prototype IoT device achieves one-year battery life for a coin battery, by streamlining the amount of sensor data to process, and by simplifying the sensory data-processing algorithms. We suggest an augmented particle filter framework by introducing a robust motion model that achieves similar accuracy despite much smaller amounts of sensor data. The evaluation results confirmed that our system exhibits a similar level of positioning accuracy as previous magnetic field-based systems, while it is more computationally and energy efficient. Although the positioning accuracy of the system is slightly lower than those of UWB- and vision light-based systems, the median accuracy of 1.6 m is sufficient for most LBS-like tasks of tracking humans in workplaces, child care services, and emergency escape services.

Bluetooth 5.0 We used a BLE chipset based on the Bluetooth 4.2 specification in the proposed system, because the Bluetooth 5.0 specification was published after its hardware implementation. Adopting Bluetooth 5.0 [54] in the proposed system would provide a larger beacon frame length, up to 255 bytes. Without the space constraints on the BLE payload size, each device would be able to deliver more information to the back-end server, which is expected to enhance the performance. In this paper, we used a highly simplified version of

PDR based on a low sensor rate (6 Hz for the accelerometer, 1 Hz for orientation), owing to the limitation of the payload size. Using a more sophisticated PDR technique (say [3]) with higher sensing rates of the accelerometer and the orientation sensor will likely improve the performance of the motion model and hence the performance of the entire system.

Deployment on Smartphone The proposed system is equipped with the same type of sensors as the ones that are used in commercial smartphones. Thus, the proposed solution can be easily deployed in smartphones while reducing the computational cost and enhancing the system's energy efficiency.

Algorithm 1: The algorithm for the estimation of heading in the particle filter framework.

Input: θ_{raw} = Raw orientation from sensor reading

Input: θ_p^{t-1} = Orientation in the previous round of each particle p

for *each particle* p **do**

  $prob$ = choose a random number between 0 - 1.0;

  if $prob < 0.4$ **then**

    θ_{path} = choose the closest orientation to θ_{raw} from the directions of the pathway where p is on;

    if $—\theta_{path} - \theta_{raw}| < 90$ **then**

      move p towards θ_{path};

    else

      move p towards θ_{raw};

    end

  else if $0.4 <= prob < 0.8$ **then**

    θ_{path} = choose the closest orientation to θ_p^{t-1} from the directions of the pathway where p is on;

    if $—\theta_{path} - \theta_p^{t-1}| < 90$ **then**

      move p towards θ_{path};

    else

      move p towards θ_{raw};

    end

  else

    move p towards θ_{raw};

  end

end

Number of Devices	CPU Usage (%)
1	5.27
10	8.52
20	19.50
30	59.50
40	71.78
50	70.82
60	87.53

Table 2.2 The CPU usage of a typical back-end server vs. the number of devices.

System	Technology	Accuracy	Algorithm Complexity	Cost	Energy Efficiency	Robustness
[21]	WiFi	2 m	Medium	Low	Poor	Moderate
[37]	UWB	39 cm	Low	High	Poor	Moderate
[35]	BLE	1.4-1.7 m	Low	High	Good	Moderate
[43]	Vision light	18 cm	Medium	Low	Poor	Poor
[5]	Magnetic	1-2.8 m	Medium	Low	Moderate	Good
[6]	Magnetic	1-2 m	High	Low	Moderate	Good
Our System	Magnetic	1.6 m	Low	Low	Good	Good

Table 2.3 Comprehensive comparison with other representative indoor localization systems.

Chapter 3

Magnetic Field based Indoor Localization System: A Crowdsourcing Approach

3.1 Introduction

As GPS signals are not available in indoor spaces, it is essential to construct a fingerprint database to provide indoor localization services. However, surveying a site to collect the fingerprints is labor-intensive and time-consuming, and the periodic site survey is usually inevitable for service maintenance as fingerprints are typically time-varying due to environmental changes in the target space.

To reduce the site survey cost, there have been many studies on crowdsourcing-based localization over the past decade [3, 12]. In the context of indoor localization, the crowdsourcing refers to a technique that constructs a database consisting of fingerprints using the measurements (e.g. WiFi signals and magnetic fields) from user devices without location labels on the site. Thus it is cost-

efficient since the system operator does not need to perform costly wardriving for collecting a large amount of fingerprint data. Also, there is no or little need of the periodic site survey.

However, the crowdsourcing-based localization systems usually exhibit lower positioning accuracy than the ones built based on explicitly surveyed fingerprint data. When constructing a fingerprint database with crowdsourced data, the estimation of the measurement locations is required since there is no location label in the measurement data [28].

Localization systems such as [13, 15, 19] leverage radio signals (say, WiFi) as crowdsourcing data. However, the radio signals are not stable due to fading and environmental changes such as human movements, changes in the physical space, and WiFi AP changes. Thus, the performance of radio- and crowdsourcing-based localization systems may not satisfy the expectations. As an alternative, the techniques using the inertial sensors including gyroscopes, magnetic compasses, and accelerometers have been suggested [3, 14]. However, using only the inertial sensors to construct the fingerprint database is risky, mainly due to heading (direction) errors caused by the magnetic disturbances in indoor spaces. We thus leverage the inertial sensors as a supplementary role to enhance the localization performance.

In this paper, we design an indoor localization system using the crowdsourced fingerprints of magnetic fields. The steel structures of a building result in distinct patterns of the magnetic fields at individual points in an indoor space. The indoor positioning techniques such as [2, 6, 7] leverage such patterns as magnetic fingerprints. It is well known that (e.g. [2]) the magnetic fingerprints are robust to the environmental changes, and nearly unchanged as time goes on. Localization techniques such as [12] propose to rely on crowdsourcing magnetic fingerprints. Based on the graph modeling, [12] suggests a clustering

methodology for the crowdsourced fingerprints based on the corridor length, the average heading direction, and the similarity among the magnetic fingerprints. However, the learning time increases in crowdsourcing scenarios since [12] relies on the dynamic time warping (DTW) algorithm [34] with a complexity of $O(N^2)$ to compare the magnetic fingerprints. Meanwhile, we lower the complexity of the fingerprint comparing algorithm and introduce a novel learning model based on the hidden markov model (HMM).

In summary, we make the following contributions.

- This paper proposes an indoor localization system using the crowdsourced magnetic fingerprints, which achieves high positioning accuracy.
- We design a novel unsupervised learning algorithm based on the HMM to increase the learning and positioning performance.
- To reduce the time for HMM learning and system stabilization, we introduce a lightweight algorithm for comparing the similarity between the magnetic fingerprints.
- Using the measurement data collected from smartphones in a 60 m $\times$ 40 m office area, experiments reveal that the proposed system achieves fast learning and high accuracy.

The rest of this paper is organized as follows. Section 3.2 introduces the characteristics of the magnetic field measurements when designing crowdsourcing systems using magnetic field fingerprints. In Section 3.3, we explain the issues in designing an HMM-based indoor localization system and introduce preliminary experiments to show the feasibility of the base model. Then we detail the system architecture in Section 3.4. Section 3.5 shows the evaluation results.

3.2 Characteristics of Magnetic Field

3.2.1 Robustness

Using magnetic field patterns in indoor spaces as fingerprints can provide some advantages in terms of robustness. The magnetic fingerprints hardly change over time [2]. Also, unlike radio signals, they are not affected by moving objects like doors and humans. It is reported that medium-sized ferromagnetic objects, such as elevators, have little or no effect on the object if the magnetic sensor (say, in a smartphone) is farther than 10cm [2, 5, 7, 8]. Thus, the magnetic fingerprints rarely change in indoor spaces unless a large-scale reconstruction is carried out or large ferromagnetic objects (such as a subway train) is passing. Such robustness is significant when designing indoor positioning techniques as it can substantially reduce the amount of measurements and the time to set up a stable fingerprint database.

3.2.2 Distinctness

A raw measurement by a magnetic sensor at a location is a three-dimensional vector: $B_{raw} = (B_x, B_y, B_z)$. For calibration (and comparison) purposes, we need to transform the 3D vector into a 2D one, which means B_x is made 0 so that its heading is aligned with the north. The transformed 2D vector is denoted by B_{hv} since it has a pair of horizontal and vertical elements. The B_{hv} is only 2D and hence multiple locations may have similar values (of B_{hv}) [26, 27], which might result in poor localization performance.

To overcome these issues, we adopt the methodology in [2], which exploits the spatial change of magnetic readings. That is, as a user walks along a corridor, the sequence of 2D magnetic vectors will be the fingerprint of the corridor in our system. In contrast, the sequence of the magnitudes of B_{raw} vectors becomes

the fingerprint in [2]; the magnitudes are one dimensional, which will be less distinct.

3.2.3 Diversity issues

Magnetic readings are robust to the environmental changes; however, we need to take into account a few external factors: device diversity and user diversity.

Device diversity

Different magnetic sensors may be manufactured with different sensing methods and/or materials. Thus, different magnetic sensors may output different readings at the same location. As reported in [7], there can be absolute differences between the magnetic readings from different sensors. However, the (spatial) changing patterns of the magnetic reading along the same corridor are almost the same even with different devices. Thus, the device diversity can be easily resolved by considering spatial patterns [6, 7].

User diversity

Henceforth, we define a magnetic fingerprint to be a series of magnetic readings along a corridor. Note that, for the same path, the different walking speeds and/or different step lengths of different users may generate different magnetic fingerprints [4, 12]. Figure 3.1 shows the different patterns of the two magnetic fingerprints collected by two users with different step lengths.

To compare the magnetic fingerprints with different rates of changes, the existing systems such as [6, 12] rely on the DTW algorithm, which measures the similarity between the time series data with different time scales. However, the time complexity of the DTW algorithm is known as $O(N^2)$ where N is the

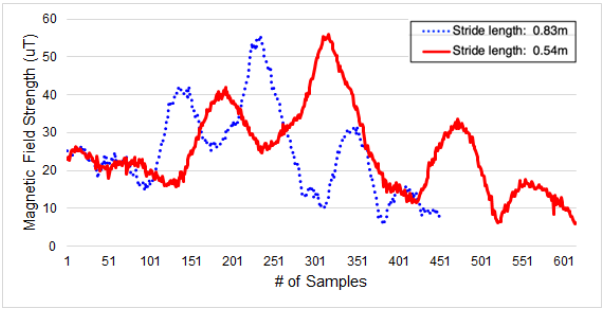

Figure 3.1 Magnetic fingerprints are plotted when two users with different step lengths walk along the same corridor. Note that the changing patterns of magnetic readings are similar even though time scales are different.

number of measurements of a series, which also spends substantial memory to look up the elements in a non-linear fashion.

3.3 Design of HMM for Crowdsoucing

3.3.1 Basic Model

The central idea of this paper is to use the Hidden Markov Model (HMM) for constructing a magnetic fingerprint database using crowdsourced data. The HMM [30, 31, 32] is an efficient machine learning model by which we can break down a system of state transitions in terms of hidden *states* and visible *observations*, and infer the corresponding states from the observation sequences. In a crowdsourcing-based fingerprint construction, we should estimate the location at which each fingerprint is collected. For this purpose, we formulate the crowdsourcing-based localization problem as an HMM in which we define the location (i.e., a corridor) of fingerprint collection as a state and the collected fingerprint as an observation.

Figure 3.2 shows the HMM-based learning model to construct a magnetic

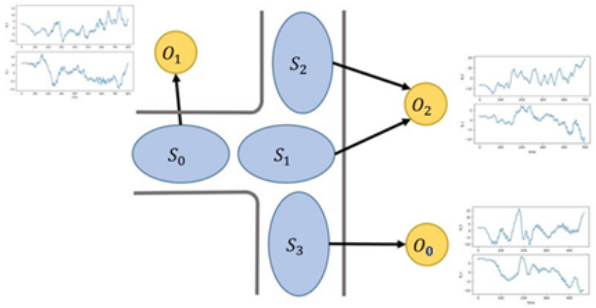

Figure 3.2 An HMM-based learning model using magnetic fingerprints is illustrated, which has 4 states and 3 observations.

fingerprint database using the crowdsourced fingerprint data. As explained in Section 3.2, the magnetic readings in indoor spaces are robust to the environmental changes. However, we have to use the spatial change of B_{hv} as a magnetic fingerprint since a magnetic reading at a location is not so distinct. A sufficiently long distance is required to use the spatial change of B_{hv} as the magnetic fingerprint. That is, the state, which models a portion of a possible path, needs to be long enough to be distinct. In an indoor space consisting mainly of corridors, we can easily define states by dividing the whole space into corridors (or their segments). Figure 3.2 illustrates 4 states: S_0, S_1, S_2, S_3, each of which is a part of a corridor in the space[1].

In Figure 3.2, O_0, O_1, O_2 show the three observations; these are three distinct magnetic fingerprints, each of which is the spatial changes of B_{hv} along the corresponding corridor. Each observation can be made in any of the states; in other words, an observation has the emission (observable) probabilities from all

[1]The possible directions in which users move along a corridor is two, say eastward and westward, or northward and southward. That is, for a given part of a corridor, two states with opposite directions are allocated. Thus, there are actually eight states for a real HMM in Figure 3.2. For now, let us proceed with the 4 states for sake of exposition

the states in which it can be observed. For instance, O_2 is observed in states S_1 and S_2. In this paper, we exploit pedestrian dead reckoning (PDR) events such as steps and turns to detect the transition between the states. Note that we adopt the algorithm in [25] to detect a step event and use the angular velocity from a gyroscope to detect a turn event.

For crowdsourcing magnetic fingerprints, the HMM has three parameters for learning after defining the set of the states $\Omega_X = q_1, \ldots, q_N$ and the set of the observations $\Omega_O = v_1, \ldots, v_M$, where q_i is the i-th state and v_k means the k-th observation.

$$HMM = (\Omega_X, \Omega_O, A, B, \Pi) \tag{3.1}$$

The three parameters are the transition probability A for transitions between the states, the emission probability B for the observations from all the possible states, and the initial state probability distribution Π when the HMM learning process starts. Equation 3.2 shows the relation between the parameters, where X_t and O_t are the system state and the observation at time t, respectively.

$$\begin{aligned} A &= \{a_{ij}\} = Pr(X_{t+1} = q_j | X_t = q_i) \\ B &= \{b_i(k)\} = Pr(O_t = v_k | X_t = q_i) \\ \Pi &= \{\pi_i\} = Pr(X_0 = q_i) \end{aligned} \tag{3.2}$$

In the HMM for the crowdsourcing scenarios where users move and report magnetic readings, a_{ij} means the probability that a user moves from a location (i.e. state i) to another (i.e. state j), and $b_i(k)$ refers to the probability that an observation v_k is measured in state q_i. Π refers to the probability distribution of the locations where the user starts walking in the test space. A can be allocated depending on the structure of the target space, and Π can be allocated equally for all states since users may start collecting magnetic data from anywhere. Thus, learning A and Π is straightforward. However, learning the values of B

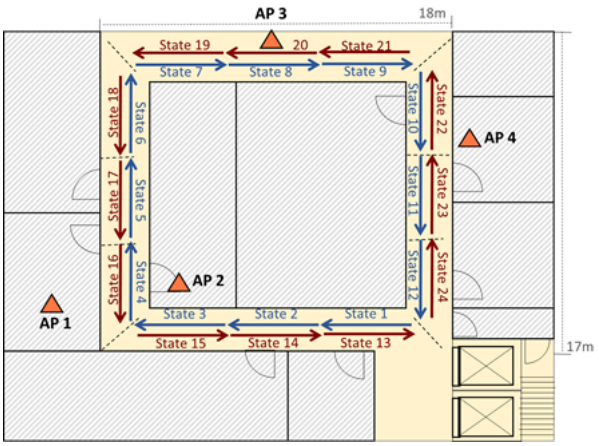

Figure 3.3 Preliminary experiments of the HMM-based crowdsourcing localization are carried out.

is not easy.

3.3.2 Issues in HMM Learning

To learn the HMM parameters, we adopt the Baum-Welch algorithm [33], which learns unknown parameters by iterated operations on the sequences of the observations, and requires $\{A_0, B_0, \Pi_0\}$ as initial inputs. Note that, the closer the initial parameters are to the actual probability distributions of the states and the observations, the higher the learning accuracy will be.

While it is easy to allocate the A_0 and Π_0, allocating B_0 is not straightforward. Since the spatial changes of B_{hv} in multiple states might exhibit similar patterns, it is not easy to assign measured magnetic fingerprints to the corresponding measured locations.

3.3.3 Preliminary Experiments

We conduct preliminary experiments (i) to show how to allocate the parameters of the HMM and (ii) to demonstrate how the HMM-based learning scheme

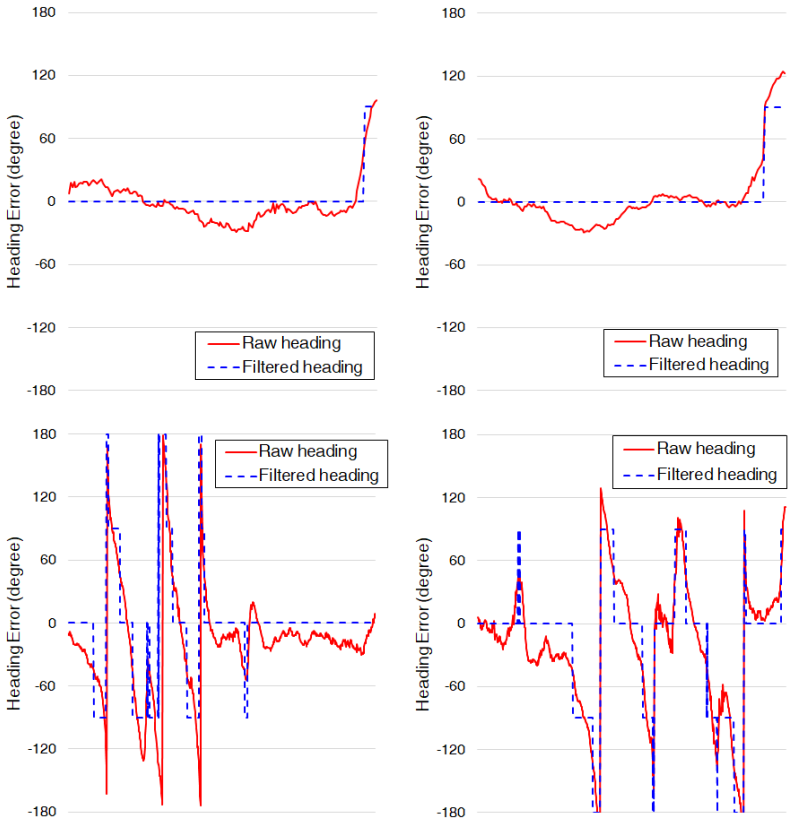

Figure 3.4 The errors of the estimated heading directions and the refined directions are plotted as a user walks along four different corridors in the testbed. The heading estimation errors are mostly marginal or intermittent; however, the bottom right case shows substantial errors due to magnetic disturbances.

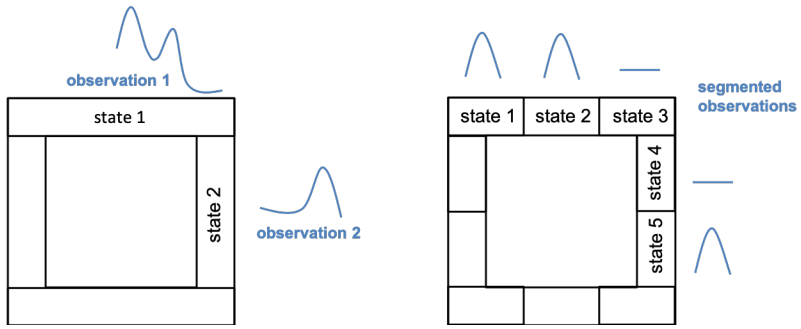

Figure 3.5 Segmentation of the state too short makes many same magnetic patterns in the target space.

performs. Figure 3.3 shows the testbed consisting of the four corridors, which stretch over a 18m * 17m space in an office building. Each state corresponds to a corridor (or its segment) of fixed length 5m. Also, the starting point of a user is set to a location like an elevator at the right lower corner for simplicity. The experiments focus on how to allocate the parameters of B_0 accurately since it is important to set the initial probabilities to achieve high accuracy in the HMM-based localization scheme.

When defining the state, the length of the state and the learning accuracy are in a trade-off relationship since the length of the state is directly related to the length of the magnetic observation. The longer the magnetic observation having high discernibility, the higher the learning accuracy. However, the longer state may not include the location for the user to move, such as corners. On the other hand, the shorter the length, the lower the discernibility of the magnetic observation. As depicted in Figure 3.5, Segmentation of the state too short makes many short and simple patterns that may be the same as the other patterns in the target space, resulting in severe low learning accuracy. Therefore, for efficient modeling, we have defined the state as moderately long and segmented in corner points.

There are two approaches when we allocate the parameters of B_0. First we can assign the same value for all the probabilities of B_0; while this is simple, the training the HMM with such initialization is likely to fail. In the second approach, every probability is set to a different value based on additional data from other sensors. For this, we use the location information of a few WiFi access points (APs) as a hint for setting initial probabilities. First of all, we collect the received signal strength (RSS) from the APs as well as magnetic fingerprints using smartphones. Also, we estimate the distances between the APs and individual states based on the Log-Distance Path Loss (LDPL) model with the WiFi RSS. Equation 3.3 shows the LDPL formula, which is a radio propagation model of the distance d from a WiFi AP to a smartphone considering its path loss $\overline{PL}(dB)$.

$$\overline{PL}(dB) = \overline{PL}(d_0) + 10nlog(\frac{d}{d_0}) \tag{3.3}$$

where d_0 is a reference distance, and $\overline{PL}(d_0)$ is a path loss at the reference distance, and n is a path loss exponent reflecting the surrounding environments. We set n as 2 and d_0 as 1m at the experiments.

For example, in case of state 1, the distances from the APs are 12m, 15m, 20m, 4m, which correspond to -61dBm, -63dBm, -66dBm, -50dBm as RSS values. RSS values at different locations exhibit different patterns depending on their distances from the APs, which can be used for allocating B_0. As mentioned earlier, there are two states for a single corridor (or its segment) since users walk in two directions. Thus the two states of the same corridor whose RSS values are most likely to be mapped to the distances from the APs will be assigned to 0.5, respectively, as the initial value of the observation probability. We use 24 states (i.e. 12 corridors), each of which is a corridor of 5m length; we identify 37 observations from the 24 states, which is collected by users with-

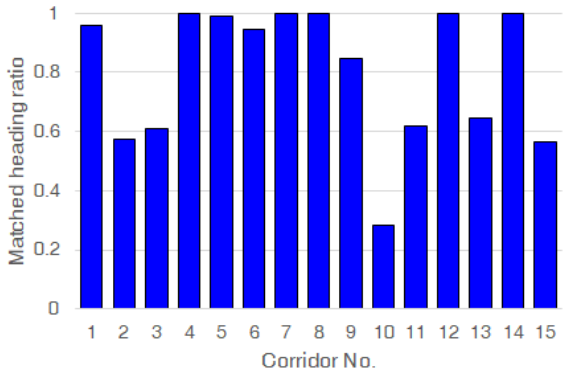

Figure 3.6 The effect of MFV filtering in fifteen corridors of the tesetbed is plotted.

out the information of their true locations[2]. Figure 3.9(a) shows the results of the Baum-Welch learning algorithm in the form of a confusion matrix, which shows the emission probability of the observation from each state. If there are multiple possible observations in a state, the sum of their probabilities is 1. There are multiple similar observations across different states since the length of the corridor is only 5m. Note that the diagonal line of the confusion matrix is not so noticeable. Nevertheless, when we input 11 observation sequences that have total 270 observations into the learning model, it shows a state-matching accuracy of 97.78%. The result is promising although we make assumptions like the knowledge of AP locations, fixed size of the corridors, and pre-determined starting points.

3.4 System Architecture

3.4.1 Enhanced Learning Model

We extend the above HMM model to relax the assumptions in the preliminary experiments such as the knowledge about AP locations, use of WiFi RSS

[2]A true location is also called a ground truth (GT) location.

Algorithm 2: *searchState* Algorithm

```
Data: O = Observations in a Observation Sequence
      S = Entire States
Result: State Sequences with the Corresponding Observations
/* initialized only at the first call                    */
o = o_1 in O, s = s_1 in S
if o.heading == s.heading then
    o.length = o.step * length_stride
    if o.length == s.length then
        add (s, o) to list_candidate
    end
    else if o.length > s.length then
        (o_f, o_b) = split(o);
        add o_b to O at the next index
        add (s, o_f) to list_candidate
    end
    if o.next == null then
        return list_candidate
    end
    else
        foreach s_n ∈ s.connectedStates do
            do searchState with (o.next, s_n)
        end
    end
end
```

values, fixed length corridors, and known starting points. In the above model with the fixed length corridors, collected magnetic readings should be divided into segments so that they can be mapped to the fingerprints of the corridors. For this, we count the steps (of a user) from the accelerometer, so that we can estimate the user's walking distance. In this way, we can identify the start and end of a fingerprint from magnetic readings.

In the extended model, a state corresponds to a corridor of arbitrary length (not of fixed length) depending on the layout of corridors. The boundary of a corridor (or its segment) for a state is demarcated by a user's turns. This

approach allows the target space to be segmented at the turning points, which helps to extract each observation (corresponding to a state) by segmenting the magnetic readings (into fingerprints) when turn events occur. For this, we need to count the number of steps and to estimate step length, to be compared against the length of a corridor during the HMM learning process. Figure 3.8 shows the floor plan of the testbed, which illustrates how the corridors of different lengths correspond to states. The blue rectangle indicates the corridors segmented at each corner. Also, the learning model does not need the additional information such as AP locations; instead it takes into account the magnetic fingerprint, the number of steps, the step length, the heading direction, the layout of corridors, to be detailed in the next section.

3.4.2 Pre-processing Crowdsourced Data

Trajectory Segmentation

In order to extract the observations from the magnetic sensor to compare against the states of various lengths, we first segment the user collected data by turns. We detect a turn event by integrating the angular velocity from the gyroscope to estimate the angle of user rotation. The threshold for the turn detection is set to 20 degrees to mitigate the effect of noises during walking. User data containing U-turns are excluded from the analysis since turn events in the middle of a corridor give wrong data to the HMM learning model.

Calibrating Heading Direction

In some cases, a user may go straight along multiple corridor segments (i.e. multiple states) if a corridor is long. Since there is no turns, we need to figure out how to identify multiple states without turns. For this, we estimate the number of steps and the heading direction of the user as additional HMM

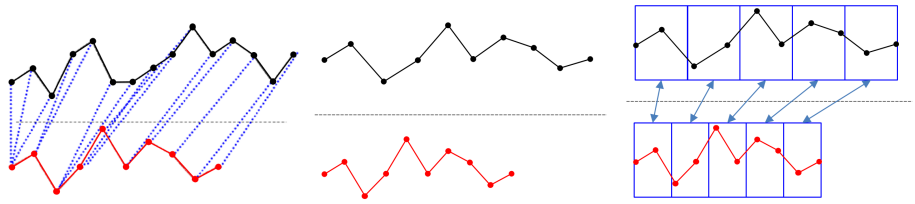

(a) Patterns with different time scales (b) Step based normalization (c) Comparing Similarity between Magnetic Fingerprints

Figure 3.7 The procedure of how to compare similarity between magnetic fingerprints is illustrated.

learning features with the magnetic fingerprint. The number of steps can be easily counted by applying the step detection algorithm [25]. However, as to the heading direction, although the magnetic disturbances in indoor spaces generate a distinct magnetic pattern at each location, they can also cause substantial errors when estimating the heading direction from magnetic readings. Each sub-figure of Figure 3.4 shows the errors of the estimated heading directions collected as the user walks along the four sample corridors in the testbed. The red and blue lines indicate the estimated heading and refined heading directions, respectively. (The refining mechanism is detailed below.) In the bottom right case of severe magnetic disturbances, there are substantial errors (even opposite direction!). However, substantial errors occur intermittently, and in most cases, relatively small errors occur.

Assuming that the user walks only in the direction of a corridor, the available heading directions of the user are constrained by the possible directions of the corridors (say, north, south, east and west). We can thus filter a small amount of heading error by dividing the 360-degree direction into the number of directions of corridors. Thus, the estimated heading direction of the user is refined into one of the four possible directions. The blue dotted line in Figure 4 shows the

filtering results; the filtering effectively reduces the heading errors.

To reduce the heading errors, we choose the most frequent value (MFV) of estimated heading directions since the severe errors do not frequently occur along the straight path. Figure 3.6 shows the results of filtering the heading directions along the 15 corridors in Figure 3.8. We choose one of the two directions in the corridor (say, east or west) and collect the heading directions while walking in a straight line since the tendencies of heading errors in both directions along the same corridor are similar. Then, the above filtering is applied to the heading directions. The y-axis means the ratio of the correctly estimated direction. Since the ratio of the correct estimation are mostly high except for corridor 10, the MFV shows the stable estimation of the heading direction.

In corridor 10, the correct heading estimation ratio is 0.28. To overcome this, we leverage the turn direction calculated by the gyroscope, which allows us to estimate the change (or turn) in the walking direction. Thus, we refine the MFV filtering results based on the gyroscope-based turn estimations when the MFV heading differences between the observations are not consistent with the gyroscope results in a user trajectory. Such turn-based direction tuning process estimates the heading directions with 100% accuracy.

3.4.3 Allocating Initial HMM Parameters

After pre-processing, we now have calibrated trajectories (or observation sequences) with the correct heading directions and the walking distances. As the number of possible sequences of states that match the user's trajectory is typically small, B_0 is mostly accurately assigned. For example, if we infer from an observation sequence that the user walks along a square path counter-clockwise, there are four possible sequences of states without the heading information. However, there is only one case if we know the heading direction.

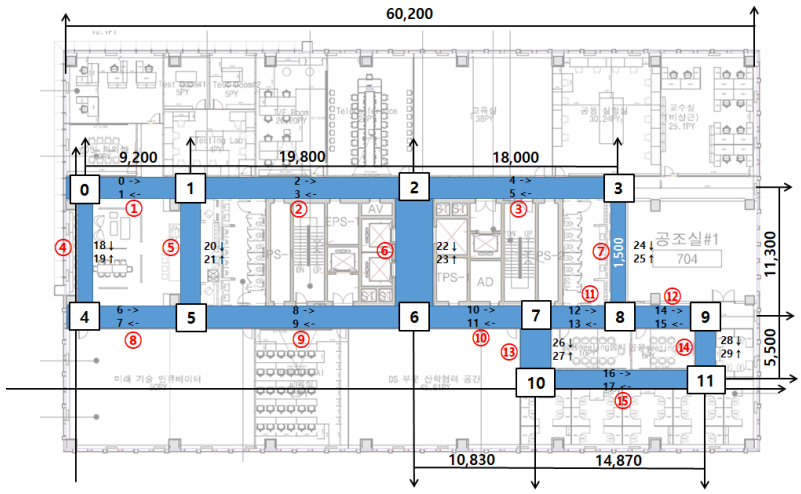

Figure 3.8 We evaluate the proposed localization scheme in an office area of 60 m $\times$ 40 m.

Algorithm 2 recursively iterates all states and finds a sequence of states whose observations match the walking distances and heading directions. The possible sequences of the states corresponding to the observations are the candidates for B_0 assignment. If a user walks along a long straight corridor, it contains a sequence of different states. In that case, Algorithm 2 splits the observation sequence considering the estimated walking distances.

The step detection algorithm achieves more than 95% accuracy. However, the walking distances of individual users can be different as their step lengths are different even if their numbers of steps are the same. For tuning the step length, Algorithm 2 is performed by adjusting the step length by 0.05m in the range of [0.55m - 0.7m]. Such fine-tuning process may generate multiple candidates for a single observation sequence. Also, if there are multiple possible sequences of corridors that match the given trajectory in the target space, a wrong state might be selected sometimes in B_0 assignment. However, the wrongly assigned emission probabilities are likely to be corrected as the observation sequences

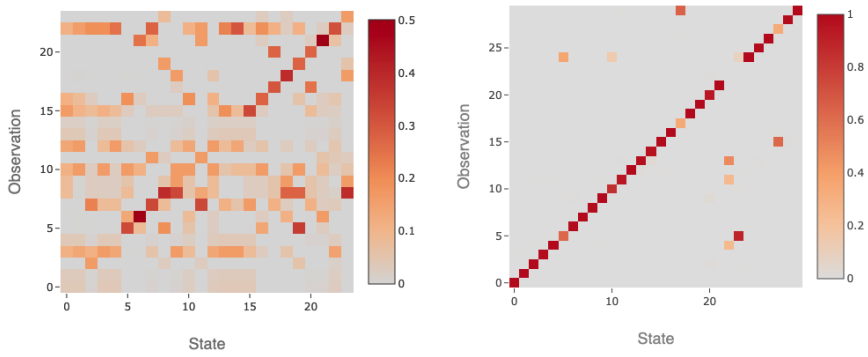

(a) Preliminary experiment (b) Extended HMM experiment

Figure 3.9 Confusion matrices of the emission probability of B after Baum-Welch learning are shown for the preliminary experiments and the extended HMM experiments.

accumulate. Thus, the Baum-Welch learning process can overcome those transient errors of the emission probabilities. In the experiments, the accuracy of state matching for the observations by Algorithm 2 is 93.3%, and further learning with the Baum-Welch algorithm during the evaluation also achieves high learning accuracy. As an alternative to algorithm 2, particle filter can also be a magnetic observation allocation algorithm based on the PDR result. We implemented the PDR-based particle filter proposed in [3] by applying 3000 particles and the MFV technique, as shown in Figure 3.10. Particle filter achieved a state matching accuracy of 94.1% for all observations, showing a slightly higher accuracy than the heuristic algorithm 2. However, the particle filter showed relatively high time complexity since 3000 particles are continuously emulated for all coordinates in the target space. Also, in corridor-oriented spaces, the abstracted magnetic observation model proposed by our HMM-based system is sufficient to design the crowdsourcing system and provide the magnetic field-based localization service.

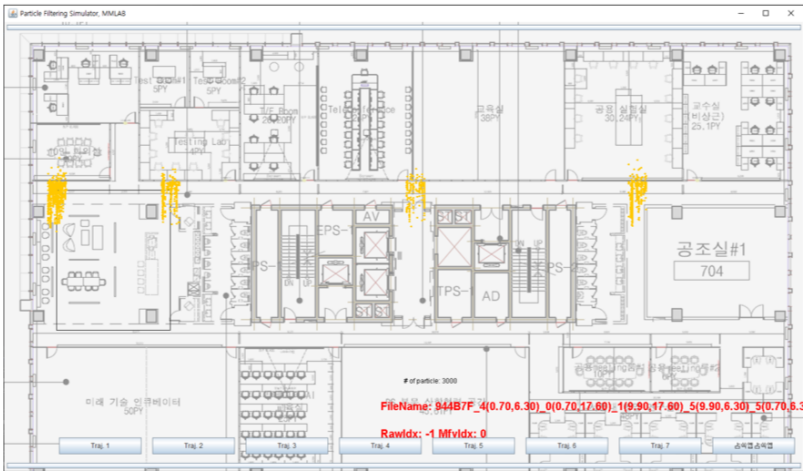

Figure 3.10 We implement the particle filter algorithm to validate the efficiency of B_0 allocation algorithm.

3.4.4 Comparing Similarity between the Magnetic Fingerprints

As explained in Section 3.2.3, DTW computes the similarity between two sequences of magnetic readings with different time scales. However, DTW becomes too slow due to time complexity of $O(N^2)$ to use in crowdsourcing systems as the sequence increases. Instead of DTW, we suggest a lightweight algorithm to compare the similarity between the magnetic fingerprints. In magnetic fingerprints, a different time scale (or walking speed) means a different reading rate.

The reading rate of the magnetic sensor is fixed per time unit; thus, the number of readings per distance depends on the user's walking speed and step length. As the walking speed is the number of steps times the step length per time unit, sampling the same number of magnetic readings per step can normalize magnetic fingerprints across different walking speeds as shown in Figure 3.7(b). As to the step length, the magnetic fingerprint can be normalized by segmenting the magnetic fingerprint into N sections as shown in Figure

3.7(c). Then we can calculate the similarity by calculating the N-dimensional Euclidean distance.

3.5 Evaluation

3.5.1 Experimental Settings

We conduct the experiments on the testbed of 60m * 40m size in an office building. The entire space of interest consists of rectangular corridors; thus there are four directions. The experiments consist of two phases. The first phase is to construct a magnetic fingerprint database by user U1 and device D1, which is carried out for 15 minutes. For this, we collect the data of magnetic and inertial sensors (of device D1) over a path of 1 km length, which consists of 6 different trajectories for Baum-Welch learning. Note that the time taken at this phase means the time to construct the initial fingerprint database. We need 15 minutes for the 2,400 m^2 sized target space and the collection time will be gradually increased in linear time as the space size increases.

In the second phase, we evaluate how accurately the proposed scheme localizes a target user over multiple trajectories (total 3.5 km length). To test user diversity and device diversity, there are 4 cases in the evaluation experiments: (1) user U1 walks with device D1 (*u1-d1*), (2) user U2 walks with device D1 (*u2-d1*), (3) user U1 walks with device D2 (*u1-d2*), (4) user U2 walks with device D2 (*u2-d2*). The whole data is collected over 41 trajectories with various lengths for three months. Note that U1 and U2 are man and woman testers with different physiques and step lengths, respectively; D1 and D2 are Google Nexus 5 and Samsung Galaxy S8, respectively.

3.5.2 Learning Accuracy

Figure 3.9 shows the confusion matrices between the states and the obser-

Metric	Dataset				
	u1-d1	u2-d1	u1-d2	u2-d2	total
P_{25} (m)	0.00	0.02	0.03	0.00	0.00
P_{50} (m)	0.18	0.38	0.29	0.15	0.25
P_{75} (m)	0.90	0.92	0.82	11.30	0.96
Average (m)	1.77	2.34	2.77	5.39	2.80
Viterbi (%)	100%	96.39%	94.92%	93.33%	96.47%

Table 3.1 Experiments to evaluate positioning and learning accuracy are carried out with user and device diversity scenarios.

vations made in each state (B) after the Baum-Welch learning for both the preliminary experiments and the extended HMM experiments. Figure 3.9(b) shows that the extended HMM experiments find B more accurately, even though the target space is more complex and the number of states is increased. The method of allocating B_0 introduced in Section 3.4.3 has improved the learning performance without the information like AP locations.

However, it is difficult to quantitatively evaluate whether the HMM learning is successful by examining B since multiple observations can be assigned to the same state. We thus evaluate how accurately B is developed by using the Viterbi algorithm [29], which returns the sequence of states having the highest matching probability for a given observation sequence. The matching accuracy of the Viterbi algorithm also implies the accuracy of updating and learning B by the Baum-Welch algorithm. The last row of Table 3.1 shows the learning performance for the test user's magnetic data from the 41 trajectories consisting of total 255 observations. The 246 observations are matched exactly, showing a high learning performance of 96.47%. Among the 4 diversity scenarios, the dataset collected by U2 using D2 (*u2-d2*) performs relatively low at 93.33%, but still shows a high learning performance. If B is developed without tuning the step length as explained in Section 3.4.3, the matching accuracy of the entire

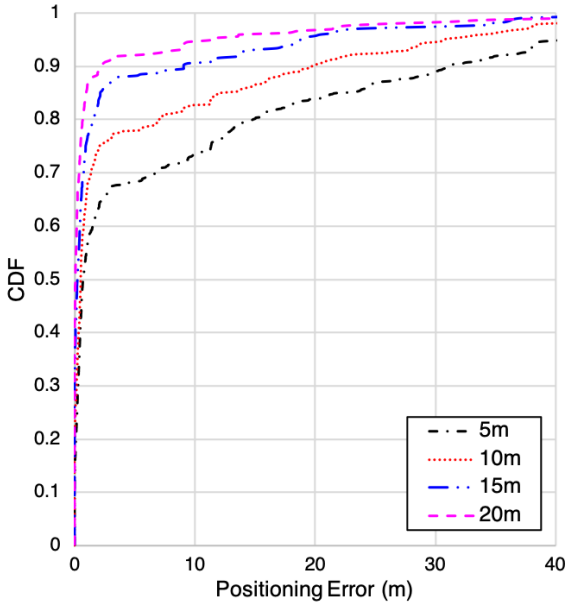

Figure 3.11 The cdf of the localization performance of the proposed scheme is plotted as we increase the magnetic fingerprint of the user in terms of the user's moving distance.

dataset is reduced to 76.56%. The learning performance heavily relies on tuning the step length during B_0 allocation.

3.5.3 Positioning Accuracy

After learning, B becomes the magnetic fingerprint database for all the states and observations. To test the accuracy of this database in terms of localization performance, we evaluate the positioning accuracy by introducing the algorithm in LocateMe [2], which accumulates some amount of the magnetic readings from user movements before requesting the localization service. LocateMe then exploits a sliding window-based method to search the magnetic fingerprint database and finds out the corridor unit with a similar pattern to estimate the user's location. Figure 3.11 shows the positioning accuracy as we

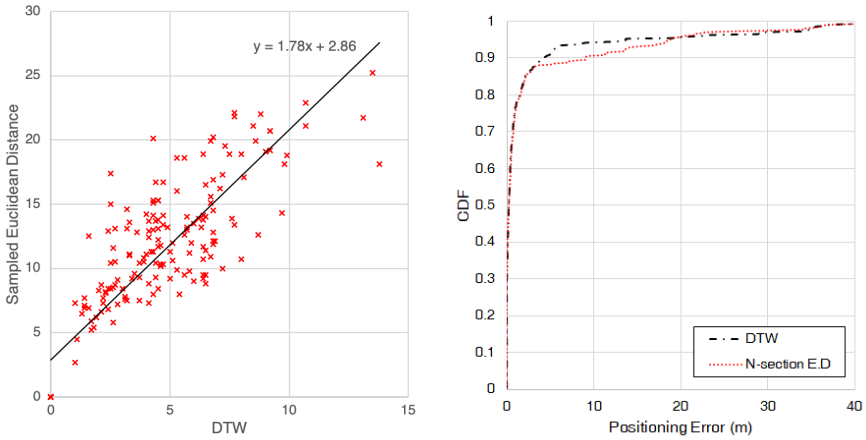

(a) Linear regression (b) Positioning accuracy

Figure 3.12 The DTW and the N-section ED algorithms are compared in terms of correlation and position accuracy.

increase the length of the accumulated magnetic readings before localization requests. The accumulated length means the minimum distance required to initiate the localization service. We set 15m as default for the minimum accumulative length. Notice that more than 90% of data show stable performance, and the users generally need 10 seconds to walk the distance of 15m. So setting 15m as the minimum distance is sufficient in the aspects of the accuracy and initialization time both.

In Table 3.1, the localization performance for the entire data is extremely high in accuracy, with an average error of 2.80m and a median error of 0.25m. For each diversity scenario, except for *u2-d2* scenarios, the positioning performance achieves high accuracy mostly. In some cases of *u2-d2*, the performance can be improved by applying matching algorithms such as Particle Filter, which reduces the fingerprint searching space. The proposed system thus shows stable and accurate localization performance and demonstrates the possibility for commercial positioning services.

3.5.4 Algorithmic Efficiency

Figure 3.12(a) shows the results of the linear regression between the similarity scores based on the DTW and the proposed N-section Euclidean distance (ED) when we compare 380 magnetic fingerprints in the dataset. The Pearson correlation coefficient of the scores of the two algorithms is 0.85, which indicates high correlation, while the proposed scheme shows much faster computational performance. The proposed scheme takes an average of 0.14ms to calculate the similarity between one pair of observations, while the DTW takes 5.63ms. Overall time delays spent on Baum-Welch learning with N-section ED and DTW are 27.3s and 9,949.8s, respectively, showing a 364x of performance enhancement. Figure 3.12(b) plots the positioning accuracy of the two algorithms in cdf, which reveals a slight difference. The matching accuracy of the Viterbi algorithm is also similar: 95.29% with DTW, 96.47% with the proposed scheme.

Chapter 4

Discussion and Future Work

4.1 Open Space Issue

As claimed in [58, 59, 60], there are still many issues to be addressed in the study of indoor localization in open space (large space). Compared to the narrow corridor-oriented space, the users can move with a higher degree of freedom in the open space. Therefore, to use the magnetic field data sharing the same dimensions globally as a fingerprint requires a massive size of searching space. Also, to provide the localization service in the open space, the administrator has to deploy many infrastructures and collect and maintain the large size of the fingerprint database to cover a wider area. In the case of the magnetic field-based system, the cost of installation, data collection, and maintenance are not problematic. There is no need for extra infrastructure to use the magnetic field, and data collection and maintenance costs can also be reduced if the crowdsourcing methodology is applied. However, in open space where users have higher freedom of movement, the temporal change over time in the mag-

netic field cannot be used as fingerprint since the magnetic fingerprint has low discernibility. Therefore, the learning model using the long and two-sided state which is based on the temporal change of the magnetic field, proposed in Section 3.4, is challenging to apply in the open space directly.

As future work, we seek to design a system leveraging landmark [62] to construct the localization database with a crowdsourcing approach. Landmark is a location where we can ensure that the multiple users passed the same location by detecting the unique pattern of sensors. In the open space with fewer spatial constraints, there is no reference point to deploy and align the crowdsourced data, and the pattern diversity and searching space of the magnetic fingerprint itself also grow wide. We thus aim to leverage the diverse and landmark points as many as possible in the open space, to find out the reference point for aligning and calibrating the crowdsourced data.

Magnetic Landmark

First, we studied whether it is possible to build a landmark using the magnetic field. If we can detect that multiple users passed the same location by using the magnetic field that is robust to changes in time and the effects of the human body, it is feasible to design an accurate crowdsourcing based system. We first collected the magnetic field data in a 39 * 67m sized open space and segmented the collected data into 0.4m sized square. Then we applied the DBSCAN clustering on all segmented data to find out the outliers. The locations with these outlier data are where having a unique magnetic pattern.

Figure 4.1(a) shows the clustering result. The black dots are the clustered points and the red dots are the outliers. We choose the rightmost outlier whose uniqueness is clear then check whether its magnetic pattern is also distinguishable. Figure 4.1(b) shows the temporal changes in the magnetic field obtained

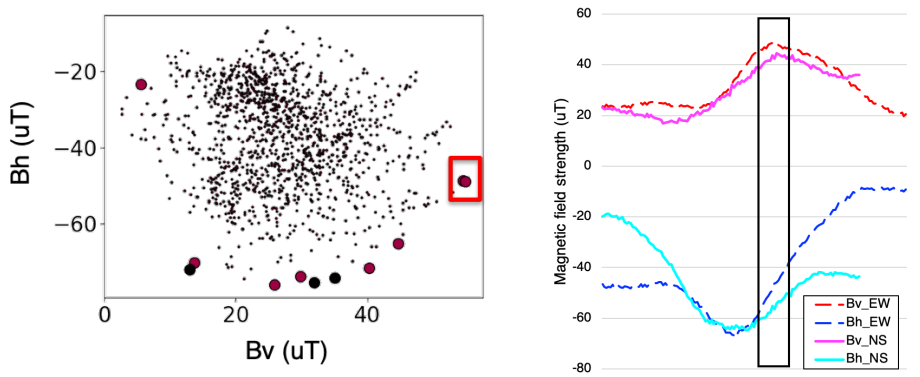

(a) Clustering result

(b) Magnetic patterns shown with different path

Figure 4.1 The clustering result to extract the magnetic landmark and its pattern with different moving path

as the user passes the selected outlier point n the east-west (EW) and north-south (NS) directions. In the open space, the same level of unique values should be observed around the magnetic landmark regardless of moving in different directions since each user passes the magnetic landmark through different paths. The red rectangle in Figure 4.1(b) means the moment when both the EW and NS paths pass through the outlier point (say, magnetic landmark), and the unique value of the rightmost point in the clustering result in Figure 4.1(a) is observed repeatedly, regardless of the walking direction. Therefore, the outlier location can be used as a magnetic landmark.

Inertial Landmark

A different kind of landmark we seek to introduce is an inertial landmark (also called seed landmark). As claimed in [1], the inertial landmark is a location where the unusual pattern is observed in inertial sensors such as accelerometer, gyroscope, and compass due to repeated walking patterns of the users. Notably,

since the locations such as elevator, escalator, stairway, and building entrance can be easily detected by the inertial sensor, we can infer and calibrate the crowdsourced positions with high accuracy by leveraging the inertial landmark if we have the floor plan of the target space. While it is difficult to know where the magnetic landmark is actually located, the inertial landmark can be used as a calibration reference point with high confidence when designing the crowdsourcing system.

System Design

The comprehensive design of the crowdsourcing system in open space to be studied in the future is as follows. First, the users collect observed inertial sensor values and magnetic patterns as they walk through the target space without recording the collection location. After receiving the collected data, the server then calibrates the user path inferred by the PDR algorithm. The raw heading direction detected by the magnetic field exhibits a significant error. The server thus combines the raw heading direction with the relative change in direction detected by the gyroscope; the overall relative path for the individual user is corrected. However, the corrected user path still contains a large absolute directional error. That is, we need to estimate how individual user paths are placed in the target space, and we plan to use the landmarks to correct these errors.

First, the server uses the inertial landmark to place the user path in the location that can be estimated with high confidence, such as elevators and escalators. Figure 4.2(a) shows an example of placing the user-collected path that is calibrated with the gyroscope, according to the location of the detected inertial landmark. We collected four paths starting from the different inertial landmarks (elevators and escalators) towards a magnetic landmark in the same

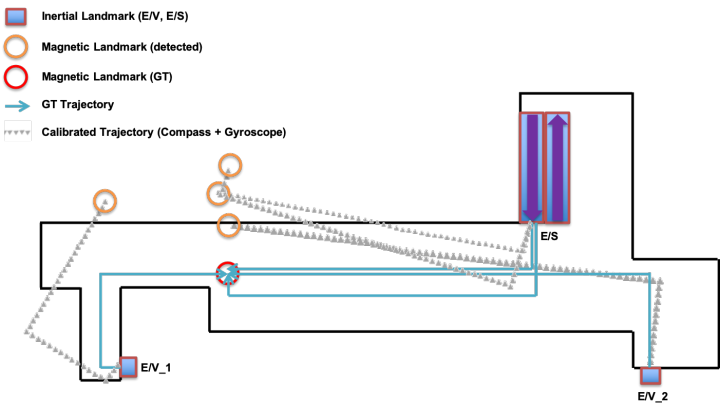

(a) Initial state

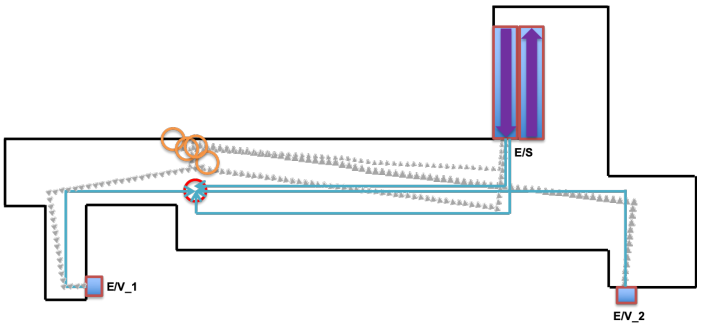

(b) Calibration with the space constraint

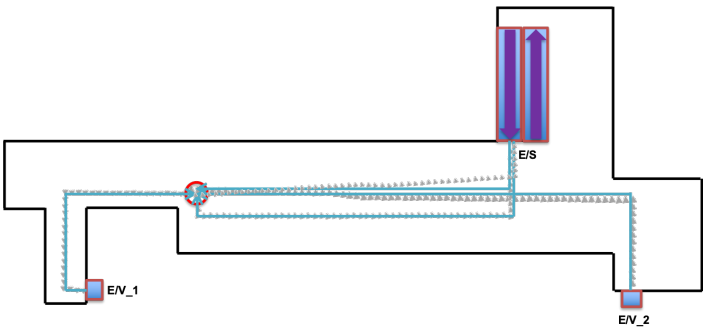

(c) Final calibration result

Figure 4.2 The suggested system design for constructing the fingerprint database using the crowdsourced magnetic field data

location. The orange circle in the figure means the location of the magnetic landmark detected on each user path, while the red circle shows the actual location of the magnetic landmark, which is not known at the point in Figure 4.2(a). Figure 4.2(b) shows the calibration result of the user's path by rotating it around the inertial landmark by applying the spatial constraint like walls. Although the open space is relatively large, the calibration using the wall is still applicable if the user path is long enough. Figure 4.2(c) shows the result of the final calibration using the magnetic landmark. By leveraging the probabilistic technique (such as maximum likelihood estimation), the server can calibrate the user path so that the locations of the detected magnetic landmark in each user path are as close as possible.

In addition to the high-level model design proposed above, we plan to address the detailed research issues. The crowdsourcing data collected by the users on various models of devices include model-specific sensitivity and the sensor errors that result from user diversity, such as differences in the type of possession of the device and the stride length. Also, since the detection accuracy of the magnetic landmark has not yet been fully verified, unlike the inertial landmark, we plan to conduct further research on whether other types of landmarks can be introduced and leveraging the statistical features to enhance the detection accuracy of the magnetic landmark.

Chapter 5

Conclusion

In the first paper, we designed and implemented a practical indoor localization system based on the magnetic field, for use in IoT applications. We first addressed the issues related to using the magnetic field for localization, and designed an IoT device equipped with a magnetic sensor, an accelerometer, and a BLE interface. Using the results of our preliminary experiments, we sought to streamline the computational overhead and the sensory data for localization. We also enhanced the efficiency of the particle filter algorithm by adopting multiple techniques. The comprehensive experiments reveal that the proposed system achieves the median localization accuracy of 1 m, while satisfying the low computational overhead and high energy efficiency requirements.

Next, we propose an indoor localization system based on crowdsourcing magnetic fingerprints. The crowdsourcing approach for indoor localization is efficient in terms of cost and time, but its accuracy is still questionable compared to the site survey-based systems. We adopt an unsupervised learning algorithm based on the HMM for better learning performance and design a lightweight

algorithm to compare the similarity of magnetic fingerprints. The proposed HMM-based localization system achieves high performance since the magnetic field is more stable than WiFi radio signals. The proposed system achieves the learning accuracy of 96.47% matching and the positioning accuracy of 0.25m median error.

Bibliography

[1] P. Bahl and V. N. Padmanabhan. "RADAR: An in-building RF-based user location and tracking system." INFOCOM 2000. Nineteenth Annual Joint Conference of the IEEE Computer and Communications Societies. Proceedings. IEEE. Vol. 2. IEEE, 2000.

[2] K. P. Subbu, B. Gozick, and R. Dantu. "LocateMe: Magnetic-fields-based indoor localization using smartphones." ACM Transactions on Intelligent Systems and Technology (TIST) 4.4 (2013): 73.

[3] A. Rai, K. K. Chinalapudi, V. N. Padmanabhan, and R. Sen. "Zee: Zero-effort crowdsourcing for indoor localization." Proceedings of the 18th annual international conference on Mobile computing and networking. ACM, 2012.

[4] F. Li, et al. "A reliable and accurate indoor localization method using phone inertial sensors." Proceedings of the 2012 ACM conference on ubiquitous computing. ACM, 2012.

[5] H. Xie, T. Gu, X. Tao, H. Ye, and J. Lv. "MaLoc: A practical magnetic fingerprinting approach to indoor localization using smartphones." Pro-

ceedings of the 2014 ACM International Joint Conference on Pervasive and Ubiquitous Computing. ACM, 2014.

[6] Y. Shu, et al. "Magicol: Indoor localization using pervasive magnetic field and opportunistic WiFi sensing." IEEE Journal on Selected Areas in Communications 33.7 (2015): 1443-1457.

[7] M. Kwak, Y. Park, J. Kim, J. Han, and T. Kwon. "An Energy-efficient and Lightweight Indoor Localization System for Internet-of-Things (IoT) Environments." Proceedings of the ACM on Interactive, Mobile, Wearable and Ubiquitous Technologies 2.1 (2018): 17.

[8] B. Kim, M. Kwak, J. Lee, and T. Kwon. "A multi-pronged approach for indoor positioning with WiFi, magnetic and cellular signals." 2014 International Conference on Indoor Positioning and Indoor Navigation (IPIN). IEEE, 2014.

[9] S. Kim et al. "Indoor positioning system using geomagnetic anomalies for smartphones." 2012 International conference on indoor positioning and indoor navigation (IPIN). IEEE, 2012.

[10] S. Beauregard and H. Haas. "Pedestrian dead reckoning: A basis for personal positioning." Proceedings of the 3rd Workshop on Positioning, Navigation and Communication. 2006.

[11] N. Mohssen et al. "It's the human that matters: accurate user orientation estimation for mobile computing applications." Proceedings of the 11th International Conference on Mobile and Ubiquitous Systems: Computing, Networking and Services. ICST (Institute for Computer Sciences, Social-Informatics and Telecommunications Engineering), 2014.

[12] H. Luo, F. Zhao, M. Jiang, H. Ma, and Y. Zhang. "Constructing an indoor floor plan using crowdsourcing based on magnetic fingerprinting." Sensors 17.11 (2017): 2678.

[13] M. Lee, H. Yang, D. Han, and C. Yu. "Crowdsourced radiomap for room-level place recognition in urban environment." 2010 8th IEEE International Conference on Pervasive Computing and Communications Workshops (PERCOM Workshops). IEEE, 2010.

[14] B. Zhou, Q. Li, Q. Mao, W. Tu, and X. Zhang. "Activity sequence-based indoor pedestrian localization using smartphones." IEEE Transactions on Human-Machine Systems 45.5 (2015): 562-574.

[15] Y. Shu, et al. "Gradient-based fingerprinting for indoor localization and tracking." IEEE Transactions on Industrial Electronics 63.4 (2016): 2424-2433.

[16] S. He, and K. G. Shin. "Geomagnetism for smartphone-based indoor localization: Challenges, advances, and comparisons." ACM Computing Surveys (CSUR) 50.6 (2018): 97.

[17] Z. Liu, et al. "Fusion of magnetic and visual sensors for indoor localization: Infrastructure-free and more effective." IEEE Transactions on Multimedia 19.4 (2017): 874-888.

[18] A. Ettlinger and G. Retscher. "Positioning using ambient magnetic fields in combination with Wi-Fi and RFID." 2016 International Conference on Indoor Positioning and Indoor Navigation (IPIN). IEEE, 2016.

[19] Y. Ni, J. Liu, S. Liu, and Y. Bai. "An indoor pedestrian positioning method using HMM with a fuzzy pattern recognition algorithm in a WLAN fingerprint system." Sensors 16.9 (2016): 1447.

[20] S. Yang, P. Dessai, M. Verma, and M. Gerla. "FreeLoc: Calibration-free crowdsourced indoor localization." 2013 Proceedings IEEE INFOCOM. IEEE, 2013.

[21] M. Youssef, and A. Agrawala. "The Horus WLAN location determination system." Proceedings of the 3rd international conference on Mobile systems, applications, and services. ACM, 2005.

[22] J. Haverinen and A. Kemppainen. "Global indoor self-localization based on the ambient magnetic field." Robotics and Autonomous Systems 57.10 (2009): 1028-1035.

[23] J. Chung, et al. "Indoor location sensing using geo-magnetism." Proceedings of the 9th international conference on Mobile systems, applications, and services. ACM, 2011.

[24] S. Suksakulchai et al. "Mobile robot localization using an electronic compass for corridor environment." Smc 2000 conference proceedings. 2000 ieee international conference on systems, man and cybernetics.'cybernetics evolving to systems, humans, organizations, and their complex interactions'(cat. no. 0. Vol. 5. IEEE, 2000.

[25] J. Chon, and H. Cha. "Lifemap: A smartphone-based context provider for location-based services." IEEE Pervasive Computing 10.2 (2011): 58-67.

[26] M. Angermann, M. Frassl, M. Doniec, B. J. Julian, and P. Robertson. "Characterization of the indoor magnetic field for applications in localiza-

tion and mapping." 2012 International Conference on Indoor Positioning and Indoor Navigation (IPIN). IEEE, 2012.

[27] B. Li, T. Gallagher, A. G. Dempster, and C. Rizos. "How feasible is the use of magnetic field alone for indoor positioning?." 2012 International Conference on Indoor Positioning and Indoor Navigation (IPIN). IEEE, 2012.

[28] B. Wang, Q. Chen, L. T. Yang, and H. Chao. "Indoor smartphone localization via fingerprint crowdsourcing: Challenges and approaches." IEEE Wireless Communications 23.3 (2016): 82-89.

[29] G. D. Forney. "The viterbi algorithm." Proceedings of the IEEE 61.3 (1973): 268-278.

[30] R. J. Elliott, L. Aggoun, and J. B. Moore. Hidden Markov models: estimation and control. Vol. 29. Springer Science & Business Media, 2008.

[31] P. Dymarski, ed. Hidden Markov Models: Theory and Applications. BoD–Books on Demand, 2011.

[32] L. R. Rabiner, and B. Juang. "An introduction to hidden Markov models." ieee assp magazine 3.1 (1986): 4-16.

[33] Z. Ghahramani, and M. I. Jordan. "Factorial hidden Markov models." Advances in Neural Information Processing Systems. 1996.

[34] D. J. Berndt, and J. Clifford. "Using dynamic time warping to find patterns in time series." KDD workshop. Vol. 10. No. 16. 1994.

[35] Y. Zhuang et al. "Smartphone-based indoor localization with bluetooth low energy beacons." Sensors 16.5 (2016): 596.

[36] J. Lee, Y. Su, and C. Shen. "A comparative study of wireless protocols: Bluetooth, UWB, ZigBee, and Wi-Fi." Industrial electronics society 5 (2007): 46-51.

[37] B. Kempke, P. Pannuto, and P. Dutta. "Polypoint: Guiding indoor quadrotors with ultra-wideband localization." Proceedings of the 2nd International Workshop on Hot Topics in Wireless. ACM, 2015.

[38] M. Kok, J. D. Hol, and T. B. Schön. "Indoor positioning using ultrawideband and inertial measurements." IEEE Transactions on Vehicular Technology 64.4 (2015): 1293-1303.

[39] C. Zhang et al. "Accurate UWB indoor localization system utilizing time difference of arrival approach." 2006 IEEE radio and wireless symposium. IEEE, 2006.

[40] L. Taponecco, A. D'Amico, and U. Mengali. "Joint TOA and AOA estimation for UWB localization applications." IEEE Transactions on Wireless Communications 10.7 (2011): 2207-2217.

[41] H. Ye et al. "Infrastructure-free floor localization through crowdsourcing." Journal of Computer Science and Technology 30.6 (2015): 1249-1273.

[42] Y. Shu et al. "Last-mile navigation using smartphones." Proceedings of the 21st Annual International Conference on Mobile Computing and Networking. ACM, 2015.

[43] S. Zhu, and Z. Xinyu. "Enabling high-precision visible light localization in today's buildings." Proceedings of the 15th Annual International Conference on Mobile Systems, Applications, and Services. ACM, 2017.

[44] C. Zhang and Z. Zhang. "LiTell: indoor localization using unmodified light fixtures." Proceedings of the 22nd Annual International Conference on Mobile Computing and Networking. ACM, 2016.

[45] S. Sen et al. "Bringing CUPID indoor positioning system to practice." Proceedings of the 24th International Conference on World Wide Web. International World Wide Web Conferences Steering Committee, 2015.

[46] T. Ozyagcilar. "Calibrating an ecompass in the presence of hard and soft-iron interference." Freescale Semiconductor Ltd (2012): 1-17.

[47] M. Siekkinen et al. "How low energy is bluetooth low energy? comparative measurements with zigbee/802.15. 4." 2012 IEEE wireless communications and networking conference workshops (WCNCW). IEEE, 2012.

[48] S. Butterworth. "On the theory of filter amplifiers." Wireless Engineer 7.6 (1930): 536-541.

[49] R. Zhang et al. "Indoor localization using a smart phone." 2013 IEEE Sensors Applications Symposium Proceedings. IEEE, 2013.

[50] D. Gusenbauer, C. Isert, and J. Krösche. "Self-contained indoor positioning on off-the-shelf mobile devices." 2010 International Conference on Indoor Positioning and Indoor Navigation. IEEE, 2010.

[51] P. Zhou, M. Li, and G. Shen. "Use it free: Instantly knowing your phone attitude." Proceedings of the 20th annual international conference on Mobile computing and networking. ACM, 2014.

[52] X. Wang et al. "Gesture recognition using mobile phone's inertial sensors." Distributed Computing and Artificial Intelligence. Springer, Berlin, Heidelberg, 2012. 173-184.

[53] Bluetooth Specification ver. 4.2, https://www.bluetooth.org /DocMan/handlers/DownloadDoc.ashx?doc_id=286439

[54] Bluetooth Specification ver. 5.0, https://www.bluetooth.org /DocMan/handlers/DownloadDoc.ashx?doc_id=421043&_ga=2.95164572 .1071486365.1502719791-975213286.1502719791

[55] KMX62-1031 Specification rev. 3.0, http://www.kionix.com/product /KMX62-1031

[56] nRF52832 Product Specification 1.0, https://www.nordicsemi.com/eng /Products/Bluetooth-low-energy/nRF52832

[57] Energizer CR2450 Specification, http://data.energizer.com/pdfs/cr2450.pdf

[58] X. Wang et al. "Received signal strength–based localization for large space indoor environments." International Journal of Distributed Sensor Networks 13.1 (2017): 1550147716686576.

[59] K. Chintalapudi, A. P. Iyer, and V. N. Padmanabhan. "Indoor localization without the pain." Proceedings of the sixteenth annual international conference on Mobile computing and networking. ACM, 2010.

[60] B. Lu et al. "WiFi fingerprint localization in open space." State Key Laboratory of Software Development Environment, Beihang University, Beijing 100191 (2013).

[61] N. Lee, S. Ahn, and D. Han. "AMID: Accurate Magnetic Indoor Localization Using Deep Learning." Sensors 18.5 (2018): 1598.

[62] H. Wang et al. "No need to war-drive: Unsupervised indoor localization." Proceedings of the 10th international conference on Mobile systems, applications, and services. ACM, 2012.

초록

지난 십수 년 동안 학계와 산업 영역을 막론하여 실내 측위 시스템이 널리 연구되어 왔다. 실내 측위 시스템을 설계할 때 WiFi, Bluetooth, 관성 센서와 같은 다양한 종류의 센서나 무선 인터페이스들을 활용할 수 있는데, 그 중에서도 지자기 센서에서 측정한 자기장의 패턴을 측위에 사용하는 시스템은 정확성과 안정성 측면에서 타 시스템에 비해 큰 장점을 지니고 있다. 철골 구조에 기반하여 건축된 현대 건축물들의 실내 공간에는 지자기장의 왜곡이 발생하며 이는 곧 실내의 개별 공간들에 고유하고 안정적인 지자기 패턴을 발생시킨다. 이를 실내 측위의 맥락에서는 지자기 지문이라고 정의하는데 이 지자기 지문은 사용자의 움직임, 문과 창문의 여닫힘 등과 같은 일상적인 환경 변화에 강건하며, 특히 WiFi 등 무선 신호와 비교하였을 때 높은 수준의 안정성을 보인다.

그러나 이와 같은 안정성에도 불구하고 지자기 지문을 이용하여 실내 측위 시스템을 설계할 때에는 몇가지 고려해야할 사항들이 있다. 먼저 지자기 지문은 센서 데이터의 낮은 차원 개수로 인하여 AP 개수에 따라 데이터의 차원이 수십, 수백개에 달하는 무선 신호에 비하여 구별성이 매우 낮다. 대부분의 기존 연구들은 많은 양의 연산을 수행하는 복잡한 알고리즘과 많은 센서를 이용하여 이를 극복하였다. 또 대상 공간의 지자기 지문을 수집하기 위한 사전 조사 비용과 주기적인 지자기 지문 재수집에 드는 관리 비용 역시 지자기 지문을 사용할 때 고려해야할 문제점이다. 따라서 본 논문은 이 두 가지 문제점을 해결하는 데에 초점을 맞추어 작성되었다.

먼저 사물 인터넷 (IoT, Internet of Things) 환경에서 실내 측위를 위해 지자기 지문을 활용하는 에너지 효율적인 경량 시스템을 연구하였다. BLE 인터페이스와 센서 2개(지자기 및 가속도계)만 탑재한 새로운 하드웨어 설계 방식을 제안하였으며, 이 기기는 코인 크기의 배터리를 사용할 경우 1년 동안 동작 가능하였다.

또한 최소한의 센서 데이터만을 이용하여 강건한 사용자 보행 모델과 효율적인 알고리즘을 도입한 파티클 필터 프레임워크를 제안하였다. 직접 설계한 사물인터넷 기기와 알고리즘을 적용한 결과, 본 시스템은 낮은 계산 복잡성과 높은 에너지 효율을 보여주면서 일반적인 사무실 공간에 대하여 평균 1.62m의 측위 정확도를 달성하였다.

다음으로는 크라우드소싱 방식을 활용하는 지자기 지문 기반의 실내 측위 시스템을 제안하였다. 실내 측위의 맥락에서 크라우드소싱은 명시적인 대상 공간의 사전 조사 과정 없이 지자기 지문 데이터베이스를 구성하는 방법이다. 지난 십수년 간 실내 측위 연구를 위해 크라우드소싱 방법론이 활발하게 연구되어 왔으나, 크라우드소싱에 기반한 기존 측위 시스템은 일반적으로 사전 조사 기반 시스템보다 위치 정확도가 낮게 측정되어왔다. 크라우드소싱 기반 시스템의 낮은 측위 성능을 극복하기 위해, 본 연구에서는 지자기 기반 크라우드소싱 데이터를 사용한 실내 측위 시스템을 제안한다. 명시적인 수집 과정 없이 스마트폰 사용자가 일상생활에서 자연스럽게 지자기 지문 데이터베이스를 구축할 수 있도록 HMM 기반의 새로운 학습 모델을 구현하였으며, 주로 복도 위주로 구성된 실내 공간에서의 평가 결과, 제안된 시스템이 96.47%의 학습 정확도와 0.25m의 중간값 측위 정확도를 달성하였다.

주요어: 파티클 필터, 실내 측위, 사물인터넷, 지자기장, 센서
학번: 2012-20733